Note

Some data used in this study belongs to Geopower Basel AG. Data and concepts published in this study may not be further used without written approval of Geopower Basel AG.

AP 2000 Report

Report title:	**AP2000 report – Structural model of potential seimogenic faults**
Author(s):	**Bastien Delacou (BEG)** **Mario Sartori, geologist, CH-1966 Ayent**
Co-authors:	**Frank Philippossian (BEG)** **Jean Savary (BEG)** **Gregory Grosjean (BEG)**
Company:	**Bureau d'Etudes Géologiques SA (BEG)** **Rue de la Printse 2** **1994 Aproz** **Switzerland**
Version:	**Final Version November 2009**
Ref.:	**4355 R 2009-11-09.doc**
Report date:	**9th November 2009**

CONTENTS

1 Introduction 4

2 Local model (reservoir): induced seismicity 5

2.1 METHODOLOGY 6

2.1.1 Relationship with the stress field orientation 7
2.1.2 Focal mechanisms and seismic alignments 8
2.1.3 Multiplets 11

2.2 WORKING FAULT MODEL (FIRST INTERPRETATION) 11

2.2.1 Fault pattern 15
2.2.2 Confidence levels 16
2.2.3 Relationship with borehole fractures 17

2.3 SYNTHETIC CONCEPTUAL FAULT MODEL 18

2.3.1 Synthetic fault model 22
2.3.2 Fault pattern 22

2.4 CONCLUSIONS 22

3 Regional model (Basel area): triggered seismicity 24

3.1 METHODOLOGY-CONTEXT 24

3.1.1 Structural synthesis (data coverage) 25
3.1.2 Regional fault families (inheritance and activities) 29
3.1.3 The Basel 1356 earthquake: literature interpretations 30

3.2 FAULT MODEL 34

3.2.1 Fault pattern – relationship with regional seismicity 34
3.2.2 Selection of relevant faults for the risk analysis (confidence levels) 35

3.3 FAULT DYNAMICS 37

3.3.1 Stress field 38
3.3.2 Recurrence – slip rates: Basel-Reinach model 39
3.3.3 Recurrence – slip rates: other estimations 40

4 Conclusions 46

LIST OF FIGURES

Figure 1: Injection rates and phases, wellhead pressure and event rates during the Basel1 stimulation 6
Figure 2: Orientation of the early cloud of earthquakes, aligned on the stress field and of the total seismic sequence, latter events following discrete structures 8
Figure 3: Focal mechanisms used in this study (from Deichmann & Giardini 2009 and Häring et al. 2008) 10
Figure 4: Working fault model 12
Figure 5: Map lengths and areas of faults in the preliminary working model 15
Figure 6: Statistical orientations of interpretative faults of the working preliminary fault model 16
Figure 7: Statistical orientations of presumed natural fractures analysed from UBI log 17
Figure 8: Possible correspondence between a specific measured nodal plane (right) and a natural fracture observed in UBI image (left) 18
Figure 9: Synthetic conceptual fault model 19
Figure 10: Data coverage 27
Figure 11: Large-scale view of our structural model with seismotectonic data 32
Figure 12: Fault model in the region of interest 33
Figure 13: Selected faults for the risk analysis 37
Figure 14: Stress field quantifications in Basel1 borehole (Häring et al. 2008) 39

LIST OF TABLES

Table 1: Fault characteristics - working preliminary model 9
Table 2: Fault characteristics - Interpretative conceptual model 22
Table 3: Selected relevant faults 42

1 INTRODUCTION

The SERIANEX (SEismic RIsk ANalysis EXpert group) study was initiated by the Canton of Basel with the aim of carrying out a complete seismic risk analysis (from geology to economic/human impact and risk communication) in relation with the deep enhanced geothermal project at the Basel1 deep borehole. The study consists in successive work-packages (named AP), the first one being the AP2000 contribution, which is presented in this report. This AP2000 contribution aims at providing structural models of potential seismogenic faults, which will be used to quantify the seismic hazard (maximum magnitudes and related frequencies), in a two step approach. The first approach is dedicated to the study of directly induced earthquakes (by re-stimulation and circulation in the reservoir) and the second to earthquakes that may be triggered indirectly (by distant stress, pressure and temperature effects). Thus, fault models proposed in this contribution reflect this approach, with local fault models presented within the Basel1 reservoir (scale in the hundreds of meters range), and regional fault models presented for the whole Basel area (tens of kilometers range).

The Basel1 borehole was drilled between May and October 2006 and reached a depth of 5 km (total depth below ground surface), where granitic rocks attain a temperature of about 200°C, and are thus economically interesting for geothermal purposes. From the surface to the maximum depth, the following formations were encountered (Geothermal Explorer data; Kaeser et al. 2007):

- Quaternary: “Rheinschotter” cap (alluvials, gravels, sands, clays) – 12 m thick.
- Cenozoic syn-rift sediments: Oligocene shales, marls and sands related to the rift activity and Eocene (pre- and syn-rift) siderolithic palaeosol – 385 m thick.
- Mesozoic pre-rift sediments: Jurassic carbonates, shales and marls and Triassic evaporites, carbonates and sandstones – 919 m thick
- Paleozoic: Permian sandstones and conglomerates (764 m thick) overlaying the crystalline basement (composed by I-type granite (45%), monzogranite (45%) and monzonite (10%)).

In this hole, a section was kept open (openhole section from 4,629 m depth below ground surface) so that water could flow during the stimulation in order to enhance the permeability of the granite and make it suitable for geothermal exploitation (circulation of hot water from the Basel1 borehole, as well as from other well(s) not yet drilled). The stimulation took place in December 2006, inducing an extensive seismological activity (section 1) leading to the interruption of the project and to the decision to run a complete seismic risk analysis before resuming the project.

2 LOCAL MODEL (RESERVOIR): INDUCED SEISMICITY

To stimulate the reservoir, approximately 11,500 m^3 of water was injected at high pressures between the 2nd and the 8th of December 2006 (Häring et al. 2008). After a preliminary injection test over the first 16 hours, the injection rate was gradually increased up to 3,300 L/min, resulting in a maximum wellhead pressure of 296 bar (Figure 1). An array of six borehole sensors, installed by the operators (Geopower Basel AG) at depths between 317 and 2,740 m, as well as the recordings of several permanent and temporary ground-level stations (coordinated by the Swiss Seismological Service), enabled the detection of more than 10,500 seismic events, 3,563 of which have been located and incorporated in our study. The seismic activity reached high levels (about 200 events per hour) with the rising of the pressure and the flow rate, and so, after 6 days of continuous injection, the injection rate was at first reduced, and then five hours later the well was shut-in and finally bled-off as the seismic activity remained unacceptably high. The main event of the induced seismic sequence was of magnitude[1] M_L 3.4 with associated macroseismic intensity from IV to V (EMS98 scale) and occurred just before bleed-off on 8th December 2006 at 16h49, although the pressure had already partially diminished at the wellhead (Figure 1). It was reported by people as a short, high frequency shaking, accompanied by a loud bang similar to an explosion (Deichmann & Giardini 2009). This event was preceded almost one hour before by an event of magnitude M_L 2.7, while the first M_L>2.5 event happened earlier in the morning (M_L 2.6 at 03h06). Even two years later, the seismic activity has not returned to pre-stimulation levels (Deichmann & Giardini 2009). Three aftershocks of M_L>3 occurred on 6 and 16 January 2007 and on 2 February 2007.

The resulting reservoir, as revealed by the seismicity, has a near-vertical lens-shaped geometry that strikes NNW-SSE with a diameter of 1.2 km at depth between 4 and 5 km, resulting in an estimated volume of 35 million m^3 (Häring et al. 2008). After the shut-in of the well, about one third of the injected water volume flowed back to the surface, the remaining being either trapped in the reservoir and/or having flowed out (by following more distant permeable structures).

[1] In the context of seismic hazard, the moment magnitude M_w is used instead of the local magnitude M_L. In this study, the strength of seismic events will therefore by quantified by M_w whenever possible. Note that for the magnitude range considered here, M_w is slightly smaller than M_L.

Figure 1: Injection rates and phases, wellhead pressure and event rates during the Basel1 stimulation
courtesy of Geothermal Explorer

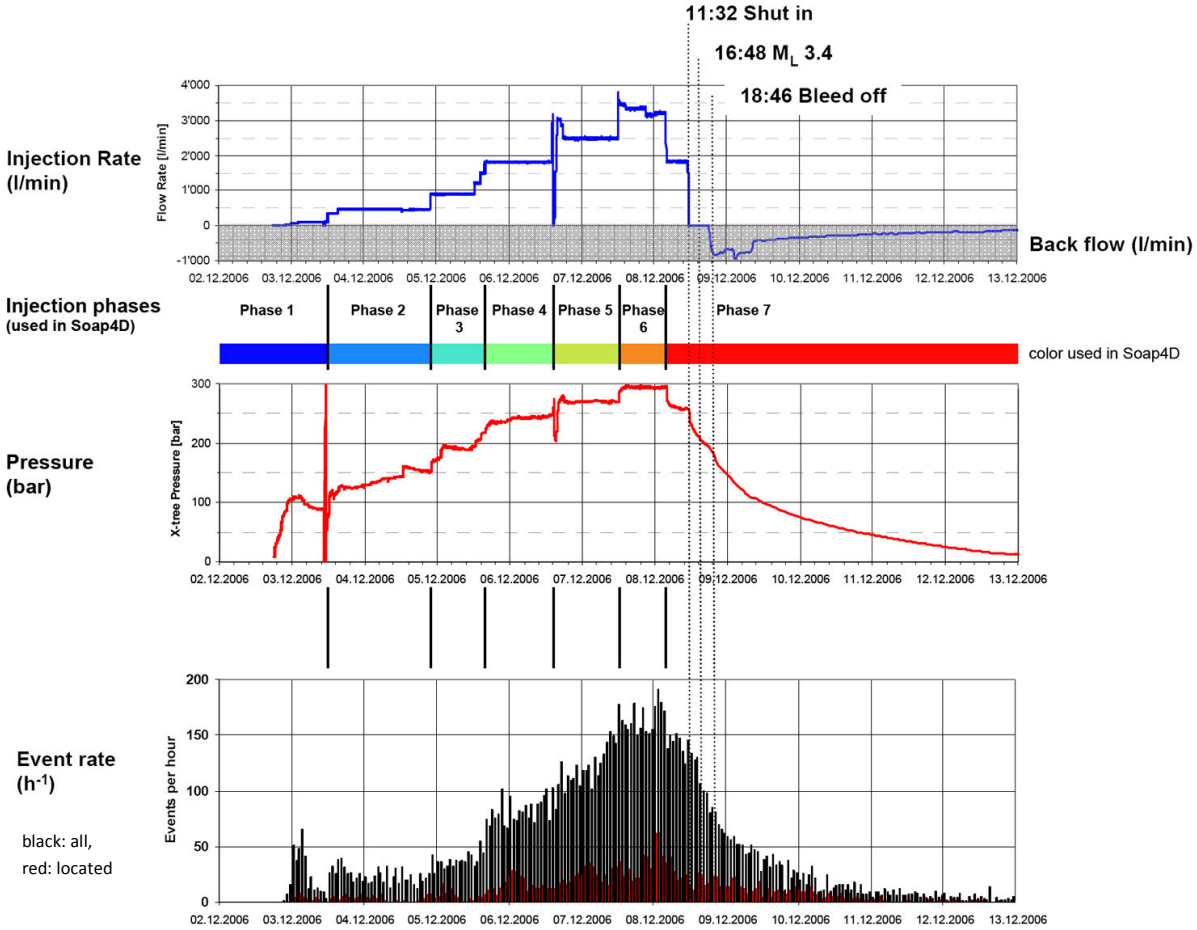

2.1 Methodology

To conceive a fault model within the reservoir, we used the available data sets presented hereafter, which mainly come from available seismicity analyses. Ultrasonic images (UBI log) of borehole fractures were also checked, but without enough clues about the persistency and the possible seismogenic nature of these fractures, they have only been used for comparison (see chapter 1.2.3).

While the induced seismic cloud can be considered as a fair image of the enhanced reservoir that was created, there is no reliable data outside this volume that can help in the interpretation of faults. Indeed, VSP (Vertical Seismic Profile) in the exploration well OTER2 was only used for estimations of depth-dependent attenuation function (Häring et al. 2008 ; Hölker et al. 2005), while P- and S- waves migration studies (Dyer et al. 2008) are poorly constrained and only give information about a possible reflection of seismic waves around the reservoir (fault or other velocity anomaly), without providing reliable data about the orientation and location of this(these) anomaly(ies). Consequently, our fault models only cover the volume affected by the induced seismicity, and no faults were interpreted outside the newly created reservoir. It is thus assumed that further stimulation aiming at extending

the reservoir size will certainly re-use the faults inside the current volume, potentially extend the current structures, but might also activate new structures which are not known yet.

To build our fault models, a dedicated 3D software was developed in B.E.G (Jean Savary), named Soap4D. It provides a clear and interactive visualization of earthquakes (with temporal evolution animations), planes (focal mechanisms), and the construction of planar faults (by regression or by "hand"). A modified version of this software (Soap4DLT, used only for visualization) can be run from the CD attached to this report (see short manual in CD file ReadMe.txt). The seismic catalog used in this software corresponds to the data set of Geothermal Explorers Ltd., whereas focal plane solutions of Deichmann & Giardini 2009 (for the 195 strongest events) are assigned to the corresponding events in the Geothermal Explorer Ltd. catalogue, without using the re-location of these authors (relative locations) in order to ensure the homogeneity of the seismic catalogue used. Also, re-located events presented in Asanuma et al. 2008 were used to study this multiplet analysis (section 1.1.3).

2.1.1 Relationship with the stress field orientation

At first glance, the seismic cloud reveals a main alignment oriented NNW-SSE (N-155°) with a smaller offsetting branch extending to the E in a WNW-ESE direction (N-100°). While the orientation of the main alignment was at an early stage considered to be oblique from the S1 principal stress direction by less than 10° (Häring et al. 2008), a detailed analysis of the evolution of the seismicity reveals a first alignment, during injection steps 1 to 4 (Figure 2; see colors and filters of earthquakes in Soap4D, see CD), even more aligned with stress directions (in the plane S1-S2). As the injection continued, the seismicity migrated outward, while the volumes activated in the first place were progressively deactivated (Kaiser effect). This outward migration of seismic activity (following the diffusion of water) followed different alignment directions: NNW-SSE to the south (N-162°) and N-S to the north, while the eastern branch appears more complicated, starting with a clear small WNW-ESE alignment and evolving into a more diffuse cloud towards the east.

While these outer alignments seem to correspond to discrete structures guiding fluid pressure diffusion, the nature of the initial stress-aligned cloud is subject to debate, as its orientation (plane S1-S2) and form (disc) correspond to what would be expected in a hydro-frac context. However, focal mechanism studies reveal the mostly shearing nature of earthquakes, even though indications of non-double couple components of focal mechanisms could explain some discordant polarities of P-wave arrivals (Deichmann & Giardini 2009). Thus, a combination of double-couple and isotropic moment tensor components with a net volume change can be proposed in this case (separate study underway, ETHZ). So, we decided to include in our models a single fault aligned on this first cloud (planes Al1 in the preliminary working model and M7 in the synthetic conceptual one) to make sure that all possible interpretations are taken into account.

Figure 2: Orientation of the early cloud of earthquakes, aligned on the stress field and of the total seismic sequence, latter events following discrete structures
export from Soap4D, see CD

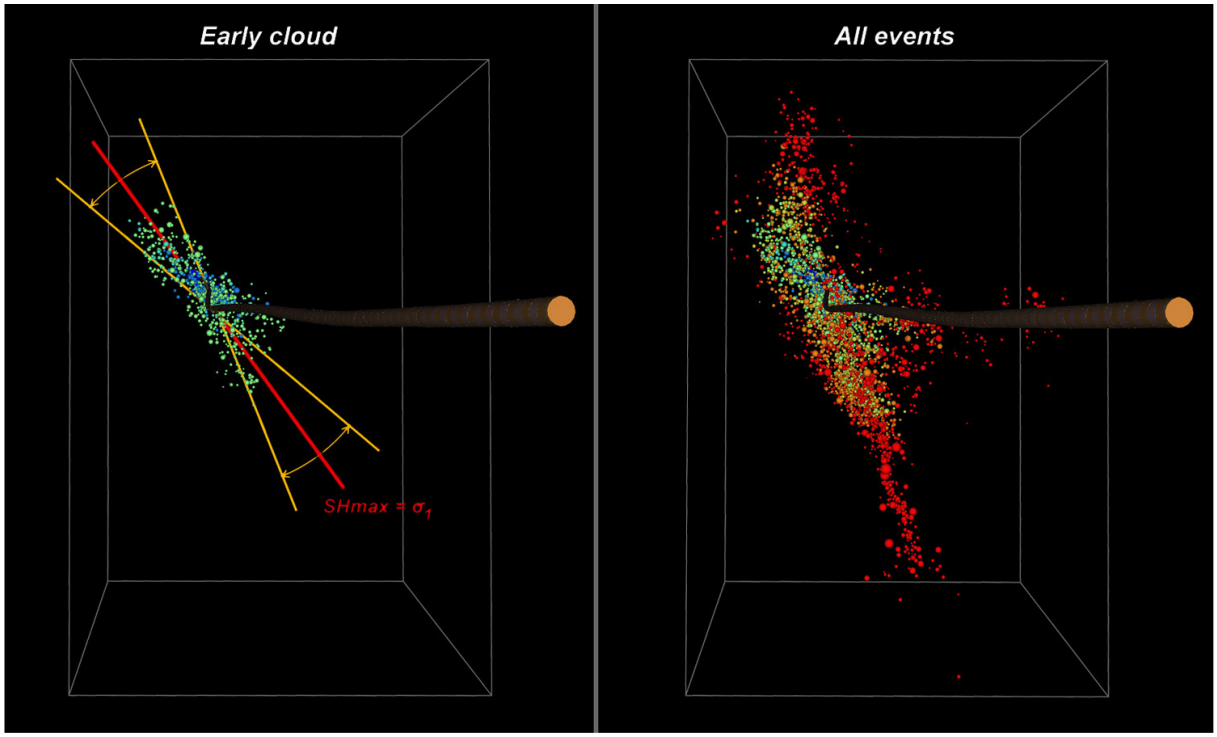

red: maximum principal stress direction, orange: uncertainty range

2.1.2 Focal mechanisms and seismic alignments

A total of 28 focal mechanisms were constructed for the strongest events (Figure 3; Deichmann & Giardini 2009, Deichmann & Ernst 2009, Häring et al. 2008). Given the large number of temporary stations installed around the epicentral area, the focal sphere is well sampled and the resulting mechanisms can be considered as well constrained. 8 of these focal mechanisms were moreover subjected to high-precision relative hypocenter localizations, which enabled the identification of the activated fault plane between the two nodal planes.

3 families of faults are defined by focal mechanisms: E-W to WNW-ESE dextral faults (4 fault planes identified by relative locations), N-S sinistral faults (4 identified fault planes) and a few NW oriented extensional mechanisms (2 in pure extension mode). Some intermediate mechanisms, between strike-slip and extension, are also observed (Figure 3). While the main alignment of seismicity is oriented NNW, focal mechanisms show slightly different orientations, with more N-S oriented planes for the sinistral family. This is particularly clear for the southern branch (see Soap4D) of the seismic cloud, which has a general orientation of N-162° while the nodal planes within it (three of which being identified by relative locations) present an oblique N-S orientation. This discrepancy has been interpreted (Häring et al. 2008) as faults organized “en-echelon” following the main alignment (Riedel structures), although a possible systematic artifact in the building of focal mechanisms (rotation of nodal planes in the N-S direction) cannot be totally rejected as an alternative cause. Another possibility is that small curvatures affect the fault plane following the main alignment,

concentrating the stresses in some bends that may correspond to the strongest events (the ones that can be subjected to focal mechanism studies). Whatever the interpretation, we tried to bring together the information from the alignment of earthquakes and from the orientation of nodal planes, in order to build a single interpretative fault plane (FM7 in Table 1) with an orientation that remains as close as possible to the nodal planes, but following the general NNW alignment. As our study aims to build a conceptual model of faults that can have a significant role in the risk study, this approach is considered more conservative than the building of several small "en-echelon" faults (that moreover cannot be spatially resolved).

Table 1: Fault characteristics - working preliminary model

Faults constructed from focal mechanisms studies

Fault ID	Confidence (%)	Nb of nodal planes (not-identified as fault)	Nb of nodal planes (identified as fault)	Events ID
FM1	30	1	0	105
FM2	80	2	3	82,94,98,108,113
FM3	40	0	1	93
FM4	70	6	0	86,103,104,147,159,162,
FM5	50	1	1	102,112
FM6	40	0	1	0
FM7	90	6	2	167,168,170,173,174,176,184,185
FM8	30	2	0	39,43
FM9	20	1	0	87

Faults constructed from multiplets analysis of Asanuma et al. 2008

Low-frequency multiplets (1-60 Hz)

Cluster ID	Confidence (%)	Nb of planes
1	20	2
4	20	1
5	20	1
13	30	1
20	20	2
22	30	1
26	40	1
41	40	1
43	20	1
45	20	1
46	20	1
49	20	1
60	20	1
72	30	

High-frequency multiplets (40-97 Hz)

Cluster ID	Confidence (%)	Nb of planes
2	20	2
9	20	1
10	10	1
41	30	1
51	10	1
62	20	1
69	10	1
98	40	1

Faults constructed from earthquakes alignments

Fault ID	Confidence (%)	Rq
AL1	30	alignments of the early cloud (phases 1 to 3)...fault or other?
AL2	40	E extension of the stimulation sequence (big branche)
AL3	30	E extension of the stimulation sequence (small branche)
AL4	20	alignment at the E termination...what plane?
AL5	30	oblique alignment (top center of the sequence)

The main M_L 3.4 earthquake of the seismic sequence, located in the lower part of the newly created reservoir, was also subjected to high precision relative localization techniques (Deichmann & Giardini 2009) showing that the activated fault plane was the WNW-ESE dextral nodal plane (Figure 3; see Soap4D). This event presents waveform similarities with several events of the same cluster, two of which presenting similar focal mechanisms, features that can be interpreted as a sequence of earthquakes occurring on the same fault plane. However a small difference of orientation exists between the dextral nodal planes, which can be interpreted as a consequence of a non-planar fault and possible differences in rakes (Deichmann & Giardini 2009). As in the previous case for the southern branch, we decided to construct a planar interpretative fault (FM2 in Table 1) that reconciles the alignment of this main-event sequence and the informations of focal mechanisms.

In the northern branch of the seismic sequence, only one focal mechanism was available (without identification of the fault plane between the nodal planes; event 105 in Figure 3). The good agreement between the N-S orientation of this part of the sequence and the N-S nodal plane of the focal mechanism leads us to construct a reliable interpretative fault plane, even if its confidence level is lowered in comparison with the previous ones (fault FM1 in Table 1).

***Figure 3: Focal mechanisms used in this study** (from Deichmann & Giardini 2009 and Häring et al. 2008)*

A: classical plan view (modified from Deichmann & Giardini 2009). Identified fault planes from high-precision relative locations are highlighted in red.

B: perspective view from Soap4D (see CD). All nodal planes in pink (two planes or one identified plane from high-precision relative localizations).

C: Rose diagram of nodal planes (gray: not-identified, red: identified fault planes).

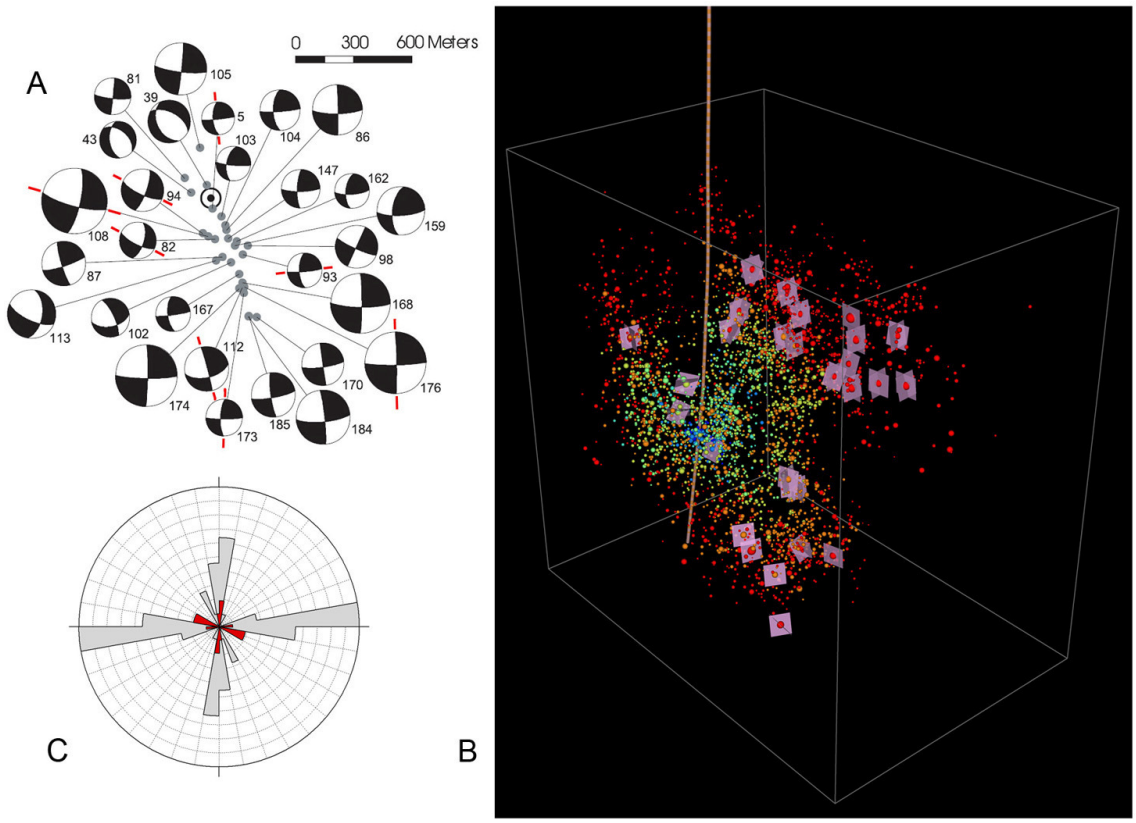

Unfortunately, no focal mechanism was compiled on the eastern branch of the seismic sequence. Apart from the obvious WNW alignment of events, a closer look reveals that the more distant eastern events are separated from the more central ones by an almost non-activated zone (see Soap4D). While the central events define a clear WNW alignment (fault AL2 in Table 1), the eastern ones have no clear spatial organization, so we propose a N-S fault plane dipping to the east (which is for us the best fitting plane) with a low confidence level (fault AL4 in Table 1).

In other parts of the reservoir, the same technique was adopted, trying to match event alignments with nodal planes of focal mechanisms (FM planes in Table 1, CD file: Faults_FocalMeca.soa). When several nodal planes appear aligned, an interpretative fault was constructed. When nodal planes have the same orientation as local event alignments, the confidence level was raised. When no focal mechanism exists but a clear alignment can be seen, a fault was also constructed (AL planes in Table 1, CD file: Faults_Alignments.soa), but with a lower confidence level.

2.1.3 Multiplets

Microseismic multiplets, which are groups of earthquakes showing similar waveforms, have been quantitatively evaluated in the frequency domain by the work of Asanuma et al. (2008). They used the first cycles of the S wave, recorded by the Riehen-2 station at depth 928 m, to evaluate similarities in both low (around or less than the corner frequency of the largest events, 1-40 Hz) and high (around the corner frequency of the average magnitude, 40-97 Hz) frequency domains. Approximately 70% of the events were grouped in multiplets: the low frequency multiplets were interpreted by the authors as “identical direction of shear slip on a single/sub-parallel macroscopic fractures” and the high frequency ones were interpreted as “repeating slip of a part of the fracture system” or “gradual rupture of one fracture”.

The hypocenter locations determined by the clustering approach of Asanuma et al. (2008) provide structural information only in a relative sense, sometimes matching information received from focal mechanisms and general seismic alignments. Therefore we have down weighted the confidence levels for the faults constructed from the multiplet clusters (Table 1).

A total of 16 faults (or fault patches) were constructed from low frequency multiplets (CD file: Faults_LFMultiplets.soa) and 9 from high frequency ones (CD file: Faults_HFMultiplets.soa), keeping only well-defined planes of events grouped as multiplets. Most of these structures were used only in the working model (section 1.2) to help analyze the coherency of other constructed faults, while the final conceptual model (section 1.3) does not contain the smallest multiplet patches (too small to be relevant in the risk analysis).

2.2 Working fault model (first interpretation)

A first working fault model was constructed from the different analyses presented in the previous section. It contains a total of 39 interpretative faults, 9 coming from the focal mechanisms analysis and events alignments, 5 from the events alignments alone and 25 from the multiplet analysis (Figure 4; Table 1; CD file: Faults_WorkingModel.soa).

Figure 4: Working fault model

A- Working fault model (perspective view from Soap4D, see CD) interpreted from events alignments, focal mechanisms (Deichmann & Giardini 2009, Deichmann & Ernst 2009; Häring et al. 2008) and multiplets regrouped events (Asanuma et al. 2008)

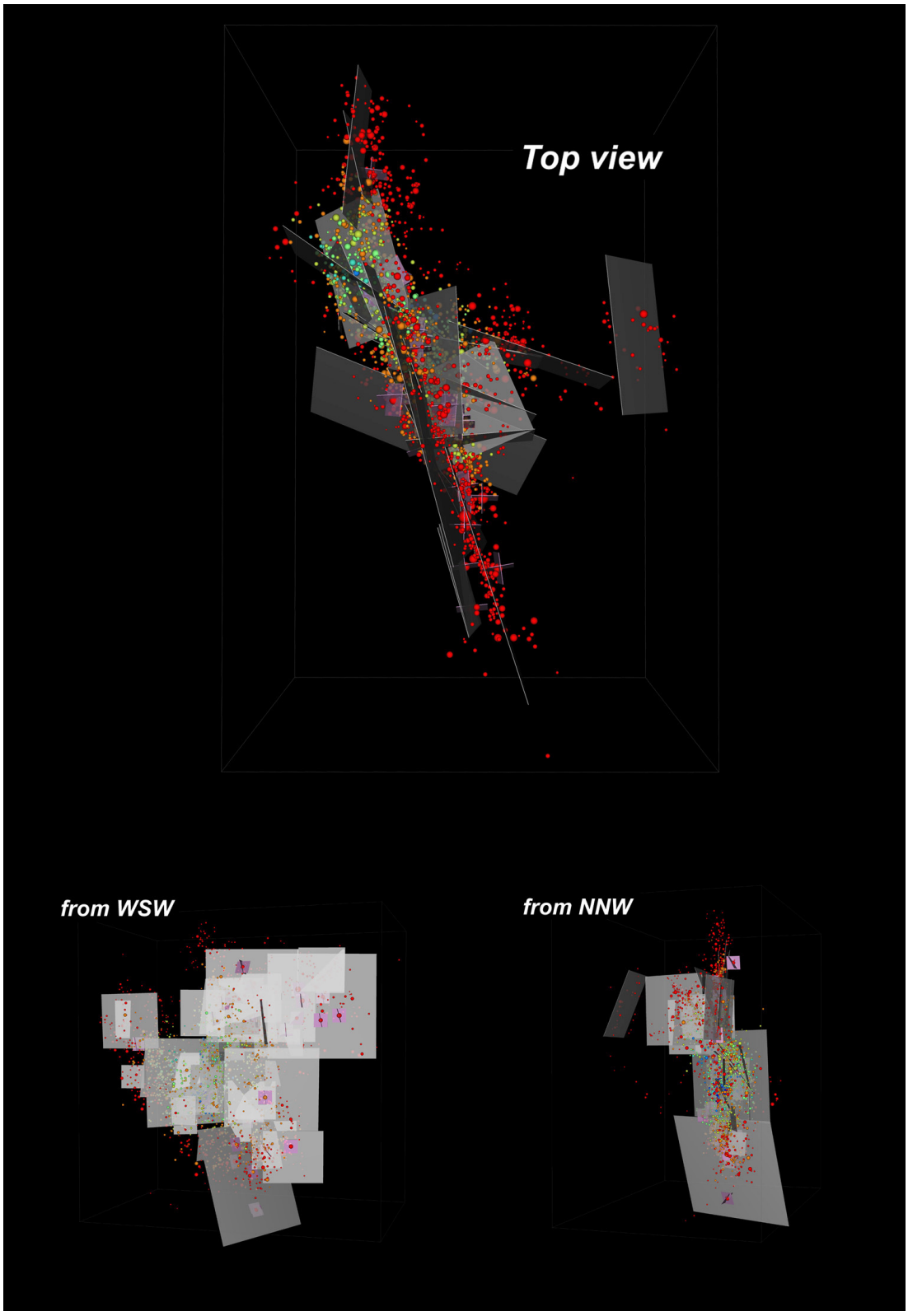

B - (continued): Working fault model - vertical cross-section in the N-75° orientation

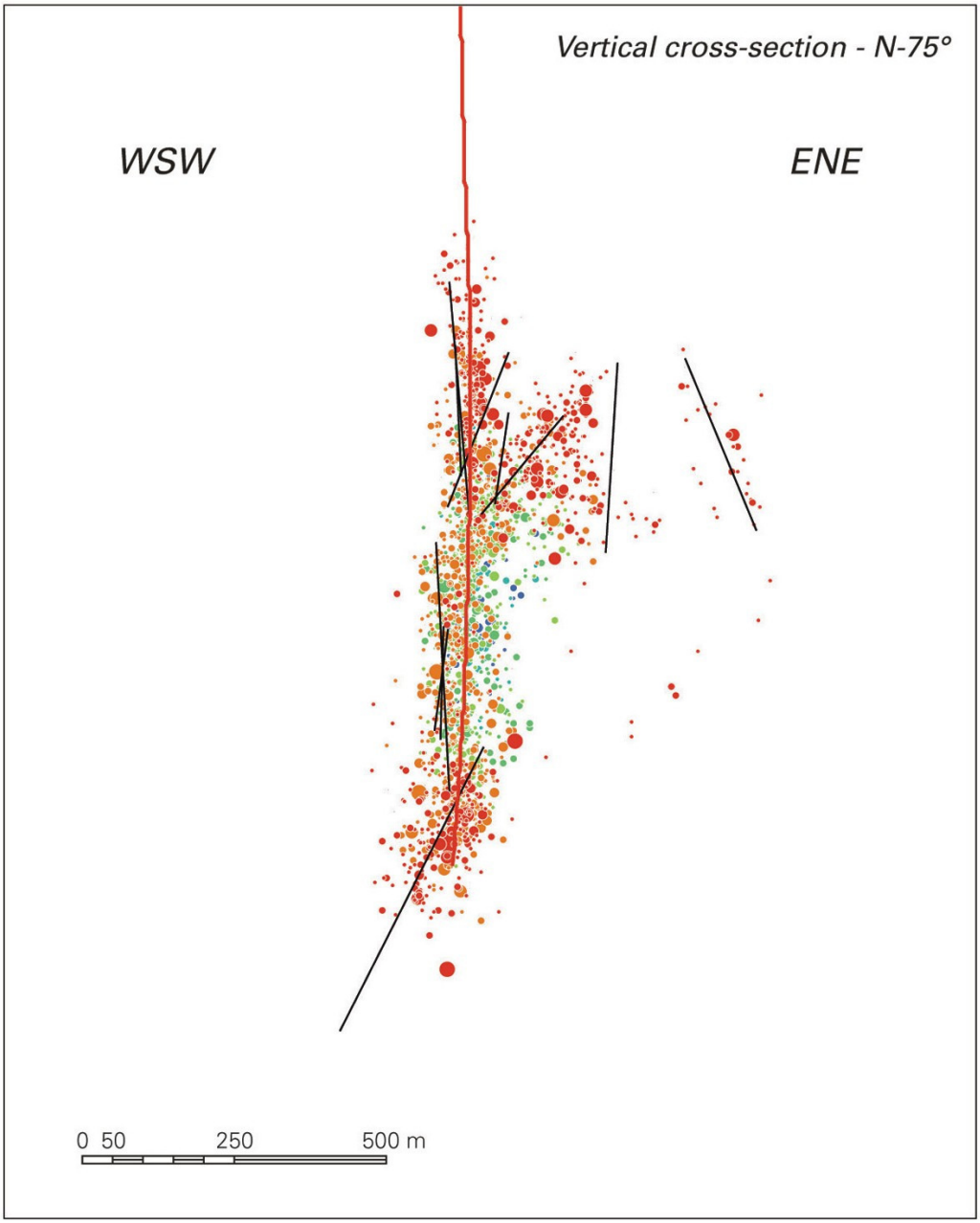

C - (continued): Working fault model - horizontal sections at 4050, 4421 and 4685 m depth

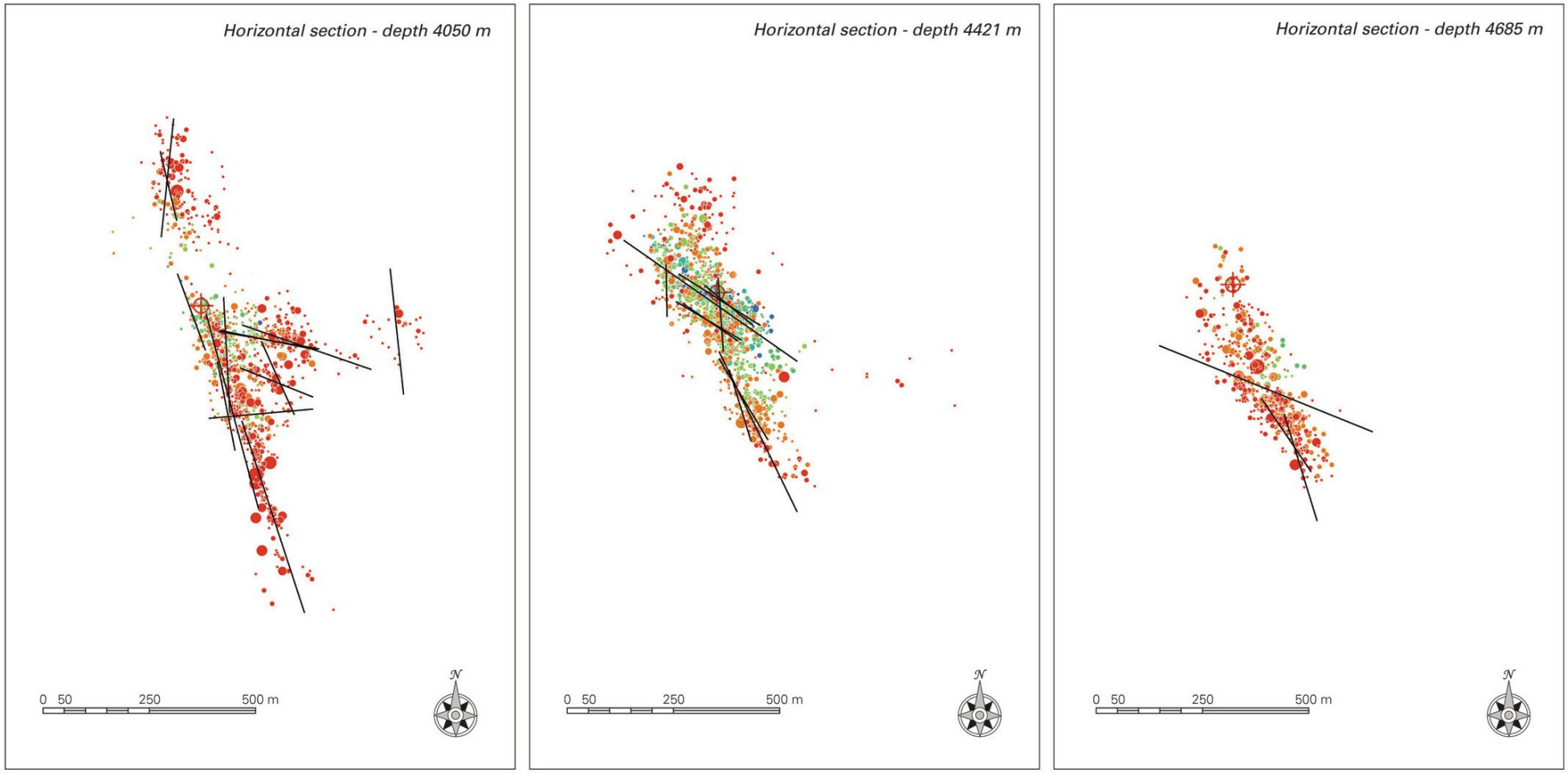

Pre-stimulation test flow outlet

Mainshock (M_L 3,4 - 8 Dec. 2006)

2.2.1 Fault pattern

Our first working model contains interpretative faults of map lengths ranging from 50 to 550 m, with a statistical maximum of about 200 m and a secondary pick at 500 m (Figure 5). The corresponding areas have maxima of about 40,000 and 250,000 m^2 respectively. These maxima correspond to the different techniques used to construct the model, smaller faults mostly coming from the multiplets analysis and small alignments of events, while bigger ones correspond to major alignments of earthquakes and related focal mechanisms nodal planes fitting.

Figure 5: Map lengths and areas of faults in the preliminary working model

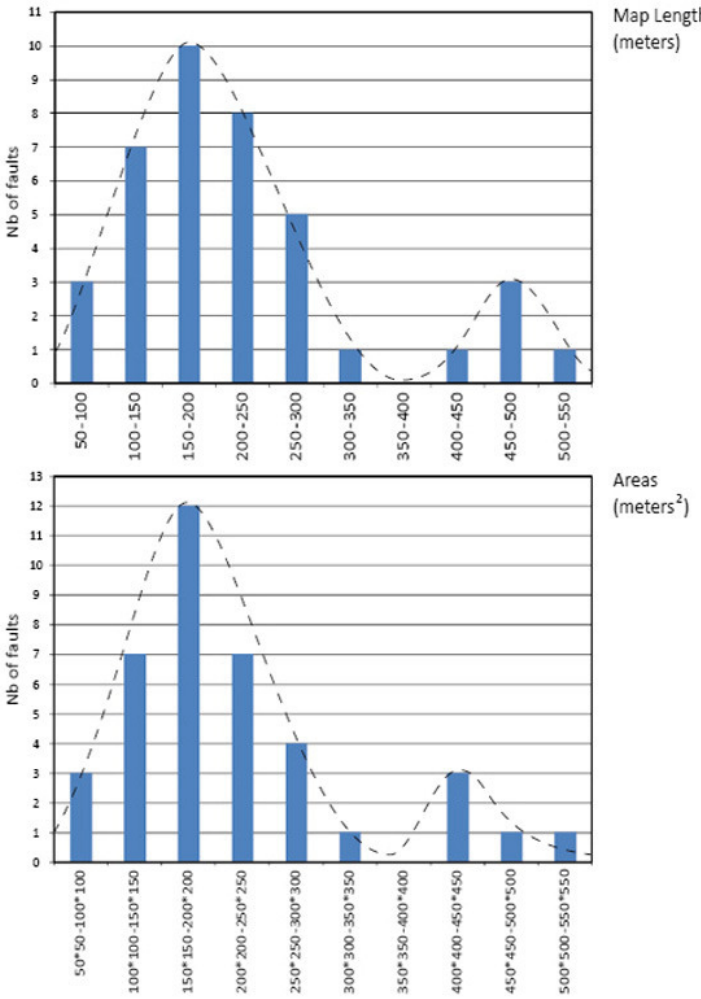

The orientation distribution shows a maximum of NNW sub-vertical faults (Figure 6), corresponding to the major alignment of the seismic cloud. As explained previously, the discrepancy between this direction and the more N-S oriented sinistral nodal planes of focal mechanisms could be related to “en-echelon” arranged fault patches inside the main alignment or to local curvature of fault planes, but one cannot totally exclude that these structures could act as single planes. So, for our risk analysis, we decided to construct the larger faults that may be activated seismically, even though additional analyses (such as

complementary (relative) focal mechanisms, as planned by ETHZ) will probably show smaller activated fault branches.

Another orientation of interpretative constructed faults is expressed by WNW sub-vertical planes (Figure 6), corresponding to the dextral planes of focal mechanisms. This family contains the fault plane of the master M_L 3.4 event in the lower part of the seismic cloud. A third group of faults are N-S, west dipping planes (Figure 6) that could be related to the few extensional focal mechanisms, even though only one of these planes has been linked to a nodal plane of this family, all other ones being constructed from event alignments.

Figure 6: Statistical orientations of interpretative faults of the working preliminary fault model

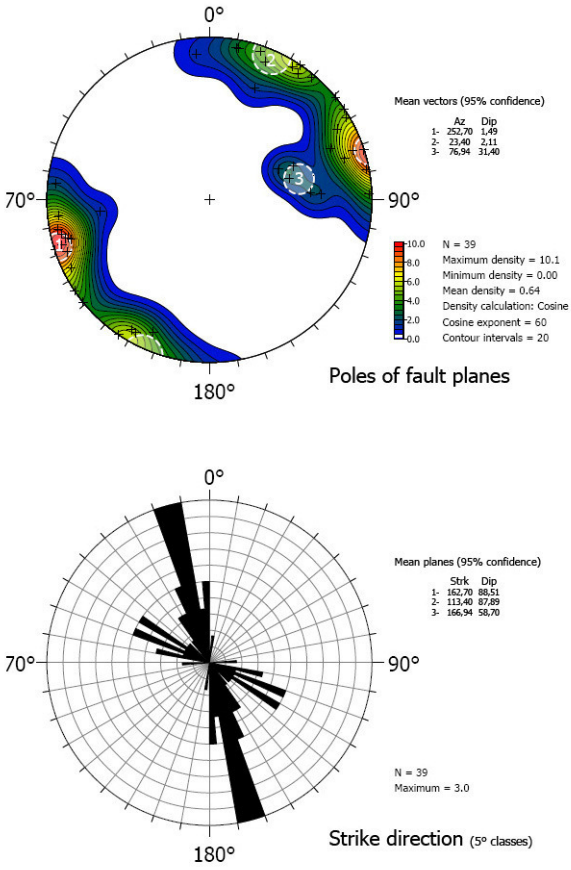

2.2.2 Confidence levels

The qualitative assessment of confidence levels was achieved by taking into account the analysis uncertainties used to build fault planes (Table 1). In general, the confidence level is high for fault planes constructed from focal mechanisms, which make up the most relevant data set indicating fault orientation, whereas the confidence level is lower for faults constructed from event alignments alone, and even lower for the multiplet-based fault planes (due to the possible artifact that may arise from this kind of analysis). More subtly, when constructed faults are related to planes of focal mechanisms chosen by relative localization, or to several planes of focal mechanisms, the confidence level is higher (FM2 or FM7 planes

for example), while planes that rely on interpretations with poor constraints are assigned lower confidence levels (such as the more easterly, east-dipping AL4 plane).

2.2.3 Relationship with borehole fractures

An analysis of UBI (Ultrasonic Borehole Imager) images was carried out in order to search for a possible correlation with faults constructed from the seismicity. The difficulty of such ultrasonic image analysis is due to the fact that the majority of fractures are drilling-induced fractures such as borehole breakouts or DITFs (Drilling Induced Tension Fractures), used to define the stress field acting in the borehole (see section 2.3.1) from the top of the crystalline basement to the borehole base. While more than 9,000 measurements were collected for drilling-induced fractures (Valley & Evans 2009), 984 natural fractures (faults, joints or diaclases) were analyzed for their orientation (Ladner et al. 2008). These fractures show an orientation distribution that is similar to the faults constructed from the seismicity, despite the fact that both datasets are of totally independent nature (Figure 7, compare with Figure 6). Indeed, the major direction trend is NNW, WNW oriented faults appearing more subtly, while a family of NE oriented faults was observed in the borehole but not in our fault model based on seismicity data.

Figure 7: Statistical orientations of presumed natural fractures analysed from UBI log
courtesy of Geothermal Explorer

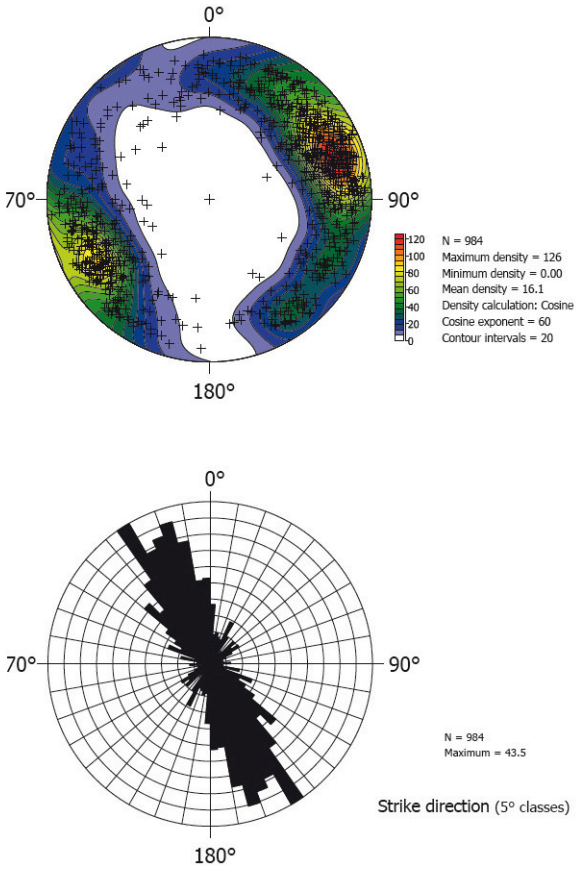

The detailed correspondence between natural faults in the borehole and the ones constructed from seismicity was checked by analyzing the intersections of modeled faults with the borehole. Only one example of a possible correlation was found, while other natural

fractures inside the borehole should be re-imaged (by another running of UBI log) to identify their possible seismic and/or hydraulic significance. The legitimate possible correlation is related to the focal mechanism of the M_L 1.7 event of 3 December 2006, studied by relative location techniques and showing an activated west dipping fault plane (event 5 on Figure 3). This event happened at an early stage of the stimulation, which explains why it is close to the borehole (less than 100 m). The intersection with the borehole is found at 4,420 m below sea level, which corresponds to a depth of 4,679 m below ground level (Figure 8). This location corresponds to a flow outlet observed during the pre-stimulation injection test (Schanz et al. 2008, Tabelle 1), while the UBI log shows a natural fracture, dipping to the SW at 4,680 m (Figure 8). We propose that the seismically-imaged fault plane might corresponds to this borehole structure, which guided most of the water flow in the pre-stimulation steps, and perhaps also during the stimulation.

Figure 8: Possible correspondence between a specific measured nodal plane (right) and a natural fracture observed in UBI image (left)

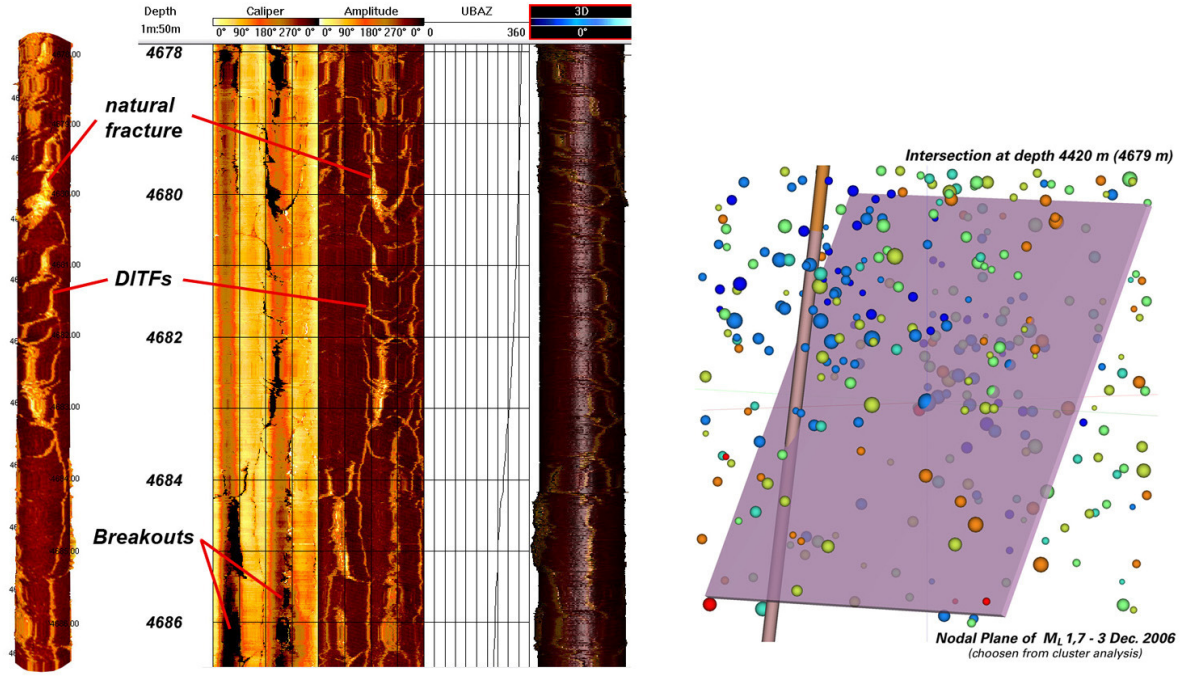

2.3 Synthetic conceptual fault model

Based on the previous working model, an interpretative synthetic model was built by merging fault patches that could belong to the same faults (Figure 9; CD file: Faults_SyntheticModel.soa). This conceptual model was built with the aim of revealing the biggest interpretable faults that could play a relevant role in the risk study. Faults are “maximized”, meaning that they may be dissected in several “en-echelon” faults. We consider this conceptual model to be a fair image of structures that may be seismically activated during another injection of water in the reservoir.

Figure 9: Synthetic conceptual fault model

A- Synthetic conceptual fault model (perspective view from Soap4D, see CD)

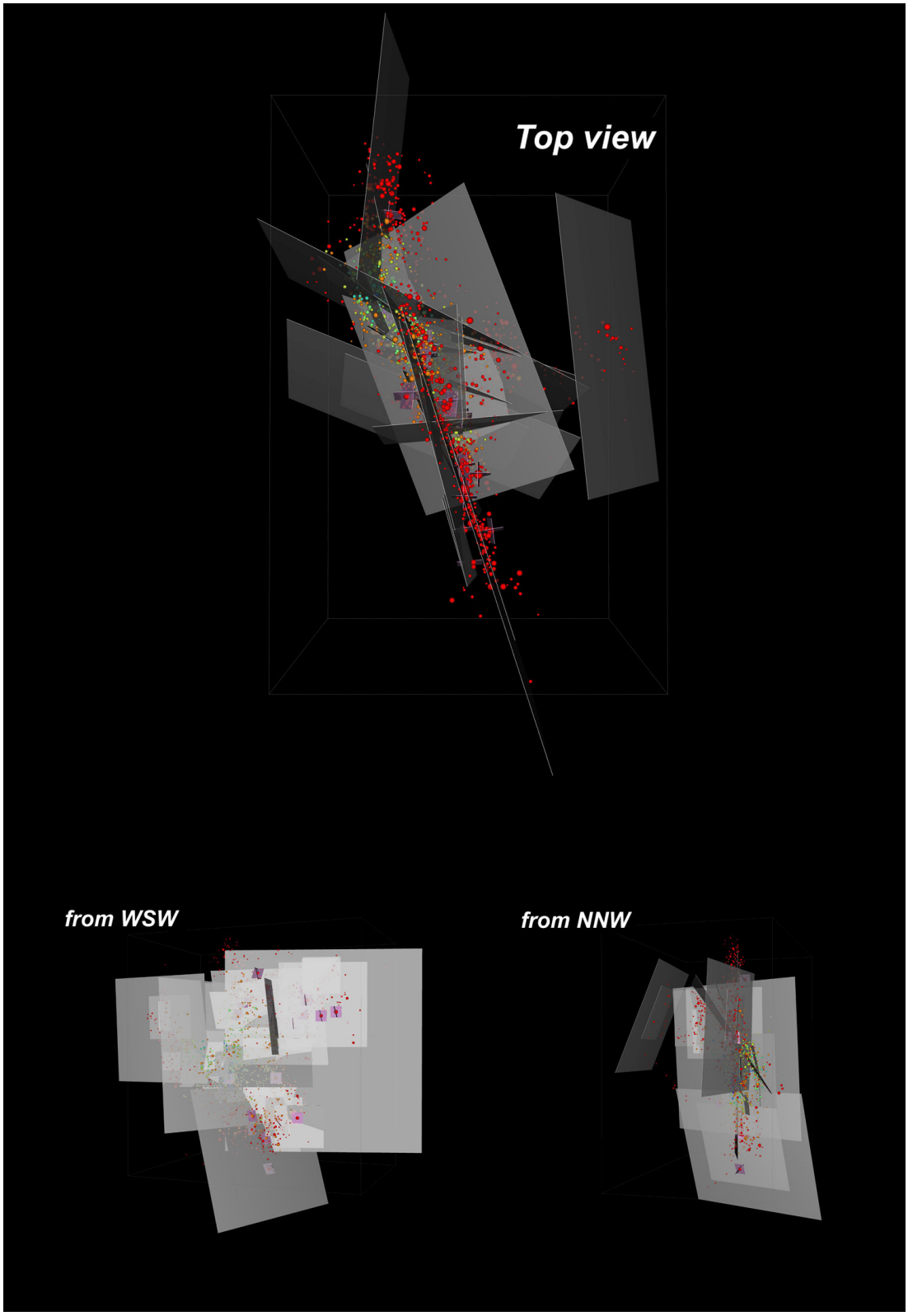

B - (continued): Synthetic conceptual fault model - vertical cross-section in the N-75° orientation

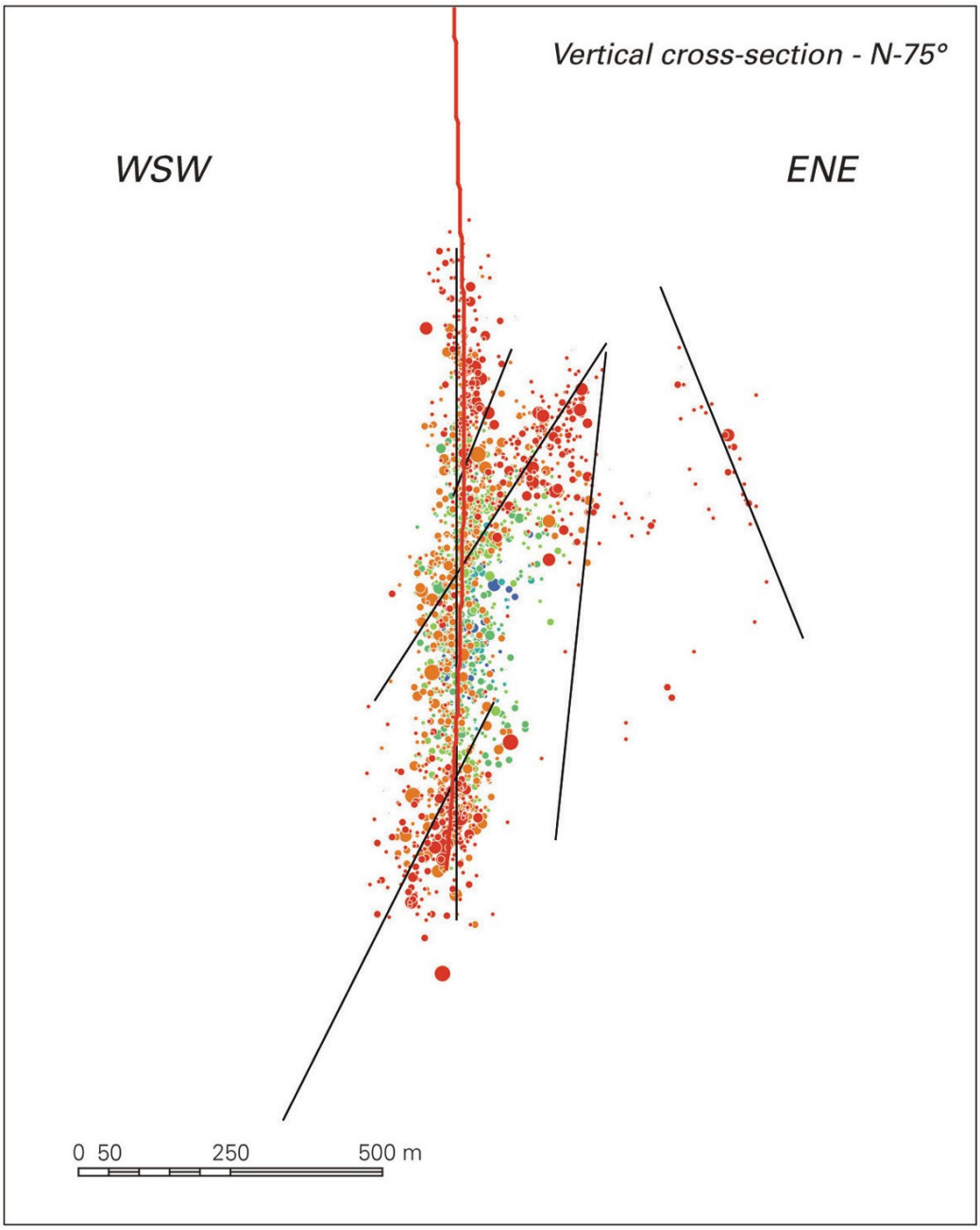

C - (continued): Synthetic conceptual fault model - horizontal sections at 4050, 4421 and 4685 m depth

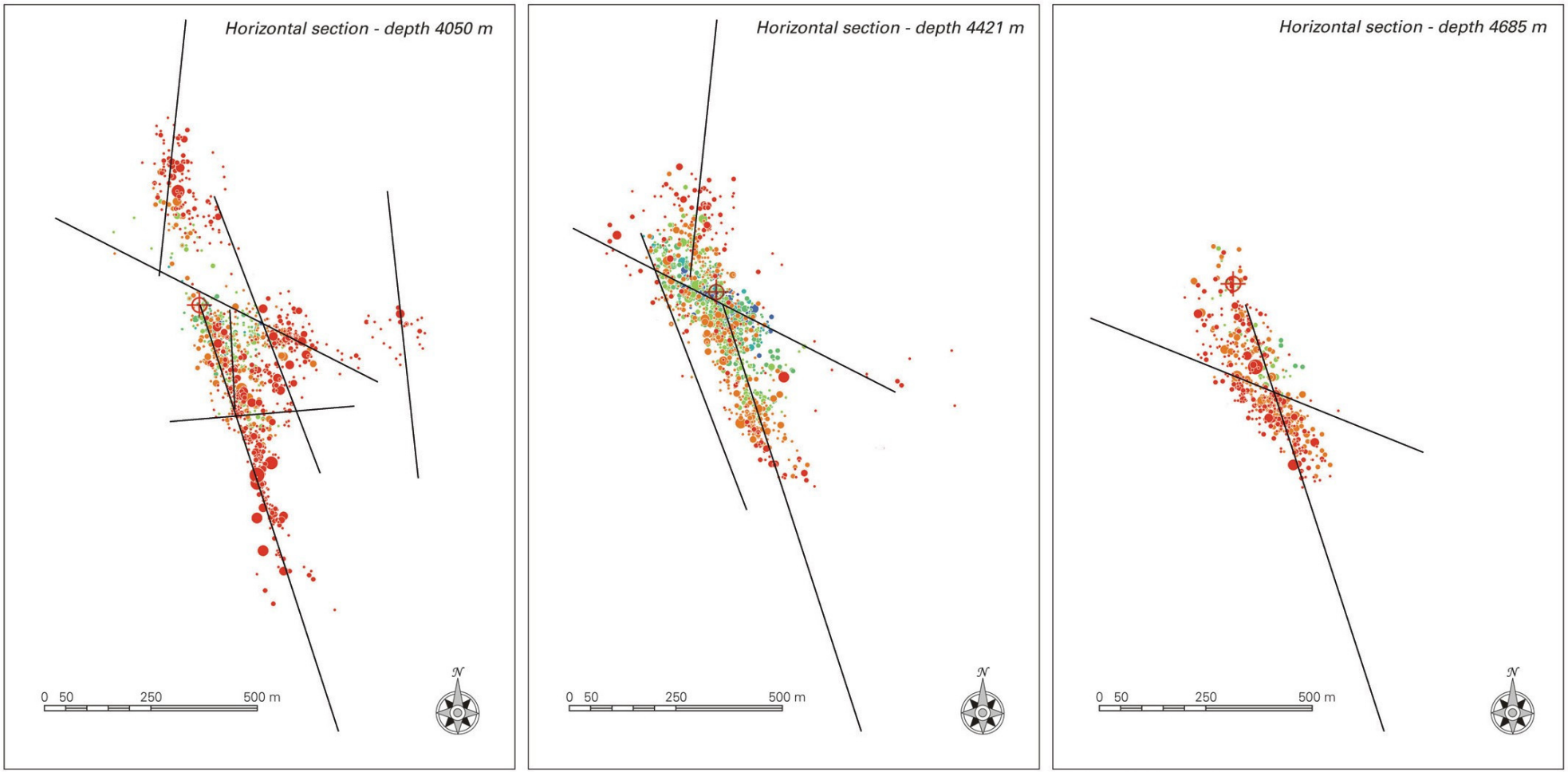

Pre-stimulation test flow outlet

Mainshock (M_L 3,4 - 8 Dec. 2006)

2.3.1 Synthetic fault model

In the first working fault model (section 1.2), some constructed faults overlap perfectly or partly with the same orientation and position: these structures can be merged into a single plane. In other places, only fault planes prolongations overlap, and a larger interpretative fault was constructed. For the more distant faults presented in the working model (southern and northern branches especially), we propose a possible outward prolongations of faults, bearing in mind that the actual extend of these structures remains unknown, because seismicity is limited to regions with elevated hydraulic overpressures.

2.3.2 Fault pattern

The resulting (conceptual) model consists of 8 interpreted faults with map lengths ranging from 230 to 1,052 m and corresponding areas ranging from 0.0579 to 1.1408 km^2 (Table 2). Confidence levels mostly relate to the rating of faults presented in the working model (Table 2, compare with Table 1), with higher confidence levels assigned to fault planes resulting from the merging of a large number of preliminary faults. Also, faults deduced from reservoir events with M_L>2.5 have higher ratings.

Table 2: Fault characteristics - Interpretative conceptual model

Fault ID	Associated plane(s) from preliminary model	Associated M>2.5 earthquake	Confidence (%)	Map length (m)	Area (km^2)
M1	FM3		40	433	0.1728
M2	FM4	M 2.5-14/12/06 (159), M 2.6-08/12/06 (86)	70	230	0.0579
M3	AL4		20	676	0.4133
M4	FM8, CIBF41, CIHF69, CIBF72, CIHF51, CIBF46, CIHF9	M 2.8-21/03/07 (184), M 3.1-06/01/07 (168), M 3.2-16/01/07 (174), M 3.2-02/02/07 (176)	90	1052	1.1408
M5	FM1, CIBF49	M 2.7-08/12/06 (105)	50	605	0.3547
M6	FM2	M 2.5-08/12/06 (113), M 3.4-08/12/06 (108)	60	840	0.5921
M7	AL1, AL2, CIHF10, CIBF13, CIBF1, CIHF2		40	846	0.6664
M8	AL5, FM9, CIBF22		30	693	0.4753

2.4 Conclusions

We constructed conceptual models of faults, mainly from seismicity data, using a two step approach: we first built a preliminary working model (Figure 4; Table 1) with all possible interpretable fault planes, and then we built a synthetic conceptual model (Figure 9; Table 2) that will be used in AP3000. As a result, 39 fault planes were constructed for the working model and only 8 larger faults for the final synthetic model, with a few faults of sufficient size to host M>4 earthquakes.

While our models can be considered as well-resolved inside the stimulated reservoir (the dataset being of high quality), one should keep in mind that no information is available from

areas outside the seismic cloud, so that non-activated faults or possible fault prolongations are bound to exist at the outer borders of the reservoir: these “hidden” structures could be activated by a further injection of water, particularly if the aim of a new injection episode is to increase the size of the reservoir, hence stimulating volumes of rock that have not yet been affected.

3 REGIONAL MODEL (BASEL AREA): TRIGGERED SEISMICITY

To compare the natural regime of seismicity with the one affected by the injection and/or circulation of water in the 5 km deep Basel reservoir, a regional model of potential seismogenic faults is prepared. This model provides the basis for AP4000 where the impact of geothermal operations on the stress state of natural faults is investigated. Therefore, a state-of-the-art model of regional faults, with estimations of dynamic properties (stresses, recurrence times of large events, slip rates), is required.

The Basel area is one of the seismically most active regions in Switzerland (Giardini et al. 2004). Even at a larger scale (Western Europe) it appears as a region of concentrated seismic activity (*e.g.* Kastrup et al. 2004; Delacou et al. 2004; Pavoni et al. 1997; Schmid & Kissling 2000; Cloetingh et al. 2006; Ziegler & Dèzes 2007), as documented by the major earthquake that took place in 1356 in Basel (strongest historically known earthquake in Europe north of the Alps), as well as by other large earthquakes that are known to have occurred since then (about ten events with magnitudes between 5 and 6 and almost 30 between 4 and 5). This activity is caused by the complex tectonic evolution of the southern part of the Upper Rhine Graben, where several tectonic phases (from the Hercynian to the Oligocene rift opening and Pliocene Jura folding) have progressively produced a zone of weakness in the European lithosphere, accumulating stresses and releasing them through significant seismic activity (Cloetingh et al. 2006). While the geodynamic setting leading to the Oligocene formation of the graben is still debated (mantle plume effect, lithosphere breaking in front of the Alps, foreland buckling, lithospheric folding ; *e.g.* Dèzes et al. 2004; Bourgeois et al. 2007), the current NW-SE orientation of shortening in this region, as well as in most West European continental areas, appears to be controlled by a large-scale interaction between the opening of the Atlantic ocean (ridge push) and the collision between the African and the European continental plates (Golke & Coblentz 1996).

3.1 Methodology-context

The goal of our regional fault model is to build a modern structural synthesis of available data, with particular attention given to structures that may play a relevant role in the risk study (based on activity, map lengths and/or orientation from the stress field). While modern synthesis were used at a large scale to provide a clear overview of fault patterns (Ustaszewski 2004; Thury et al. 1994; Laubscher 2001; Fracassi et al. 2005; Lopes Cardozo et al. 2005; Cloetingh et al. 2006; Ziegler & Dèzes 2007; Peters 2007; Tectonic Map of Switzerland 1: 500 000), various detailed analyses were also examined in order to get a more precise view of faults around the borehole (Gürler et al. 1987; Spottke et al. 2005; Huggenberger & Dresmann 2009; Ferry et al. 2005; Faber et al. 1994; Kock 2008; Geological Map of Basel 1: 25 000). These studies rely on field observations, seismic line interpretations or other geological-geophysical investigations (3D modeling, structural and seismotectonic analyses, borehole and electrical investigations, geomorphology, trenching, etc). Given the rift nature of the Southern Rhine Graben, authors have often focused their

work on extensional features (analyzing E-W sections), while compressional structures related to the neighboring southern Jura folding propagation, has also lead other authors to analyze N-S sections on the front of this recent (Pliocene) tectonic feature. This leads to an apparent contradiction because of the transcurrent nature of the tectonic regime of this part of the graben (see section 2.3.1) whereas most interpretations consider faults with vertical movements (extensive normal faults or compressive inverse ones). The result is that strike-slip faults, which are probably the most active ones today, are only poorly described in the literature, even though a reactivation of mapped extensional or compressional faults could also lead to a transcurrent regime of deformation.

One major limitation of our study is the lack of information at depth (*i.e.* below 5 km). While the surface expression of faults is well defined in outcropping areas, no investigation enables the detection of faults deeper than a few kilometers (seismic reflection profiles provide images only for the first few kilometers). Only natural seismicity occurring in the study area provides an indication of the vertical fault extension and the maximum depth where brittle failure may occur. Natural seismicity has been recorded by the German (LGRB, Landesamt für Geologie, Rohstoffe und Bergbau ; Universität Karlsruhe), Swiss (SED, Schweizer Erdbeben Dienst), and French (RéNaSS, Réseau National de Surveillance Sismique) national services. Each national service provides a separate data catalogue, whereas data catalogues for Switzerland (as of 2002) have been merged previously (ECOS catalogue, Fäh et al. 2003). In order to obtain a common data base, we have merged data catalogues provided by SED (extended ECOS catalogue; *pers. comm*. N. Deichmann), LGRB (extended LGRB catalogue; *pers. comm*. W. Brüstle), and University of Karlsruhe (*pers. comm*. F. Wenzel). To avoid redundant catalogue entries, we have associated events from different catalogues by their occurrence time. For this we assumed that events are identical if their occurrence time as listed in the catalogues does not differ by more than 10 seconds. For redundant events we used the following selection criteria:

- SED catalogue data is used for events south of 47.6° latitude,
- LGRB catalogue data is used for events north of 47.6° latitude,
- if the event is not listed in the SED and the LGRB catalogue, then catalogue data from University of Karlsruhe is used.

3.1.1 Structural synthesis (data coverage)

Based on existing information we have compiled our fault models in a GIS project (Geographic Information System). The most complete data set in the region is the synthesis compiled by Gürler et al. 1987, who study a collection of cross-sections in the Basel area on the basis of seismic lines and propose synthetic structural maps (surface, base Meeressandes, top Buntsandstein). This study has been used as a basis for the 3D GoCAD model of Huggenberger & Dresmann (2009) who additionally incorporate data from field observations and geophysical measurements (seismic lines, boreholes, electrical profiles) to better resolve near-surface structures. In contrast to the previous work of Gürler et al. (1987), the 3D model of Huggenberger & Dresmann (2009) provides an interpretation of deep fault geometries (up to 5 km). It should be noted, however, that the interpretation of deeper

structures is not well constrained by observation data. Nevertheless, we consider the model of Huggenberger & Dresmann (2009) to be the most complete and best constrained fault model for the area around Basel.

The modern synthesis of Ustasjewski 2004 (PhD thesis and related papers), more dedicated to the study of the central part of the Southern Rhine Graben (Sundgau deformation and structural inheritance in the region of La Ferette), also proposes overall graben interpretations (mostly based on the work of Gürler et al. 1987 in the Basel area for near-surface structures). This work was also complemented by a synthetic interpretation of Permo-Carboniferous trough systems underlying the Mesozoic cover (see Ustaszewski 2004 for a complete reference list). These troughs, studied in detail to the east of Basel in the southern Black Forest area by Thury et al. 1994, represent a major inheritance in the Southern Rhine Graben, controlling the geometry and position of the front of the Jura fold and thrust belt and connecting the Rhine Graben to the Bresse Graben by a continental transform zone system (Rhine-Bresse Transfer Zone, also referred to as the Basel-Dijon transfer zone in Laubscher 2007). Thus, the southern limit of the graben, flagged at the surface by the occurrence of the last frontal Jura folds, is marked at depth by a horst high in the Permo-Carboniferous, whose northern flank gave rise to an important deposition of Permo-Carboniferous sediments in a semi-graben structure, encountered in the Basel1 borehole (764 m thick).

The data set was complemented by other regional syntheses (NAGRA tectonic map of Thury et al. 1994, Tectonic Map of Switzerland 1: 500 000, Fracassi et al. 2005, Cloetingh et al. 2006, Laubscher 2001, Ziegler & Dèzes 2007, Lopes Cardozo et al. 2005) and more local geological information (Geological Map of Basel 1: 25 000, Spottke et al. 2005, Faber et al. 1994), while other works studied more specifically the current activity of faults on the basis of geomorphologic observations (Kock 2008, Fraefel et al. 2006, Ferry 2004), or fault offsets in recent deposits (Bertrand et al. 2006, Meghraoui et al. 2001, Ferry et al. 2005), providing important indications about the dynamics of faults. Given the urbanized nature of the region of concern and the concealment of structures beneath Quaternary deposits, some distant indirect information about fault patterns of the Upper Rhine Graben and adjacent areas (Nivière et al. 2008, Peters 2007, Hann & Sawatzki 2000, Cloetingh et al. 2006, Schwarz & Henk 2005) were also taken into account in order to verify the coherency of our model.

A detailed map displaying all information sources (cross-sections, seismic lines, boreholes, structural and geological maps) was compiled and serves to identify areas covered with data (Figure 10). Thus, one can quickly see where faults have been observed, and where the information is more interpretative. More importantly, we used this data coverage map to propose fault prolongations where no data had been acquired.

Figure 10: Data coverage

A - Blue dotted lines: seismic lines, black dotted lines: cross sections, crosses: deep boreholes

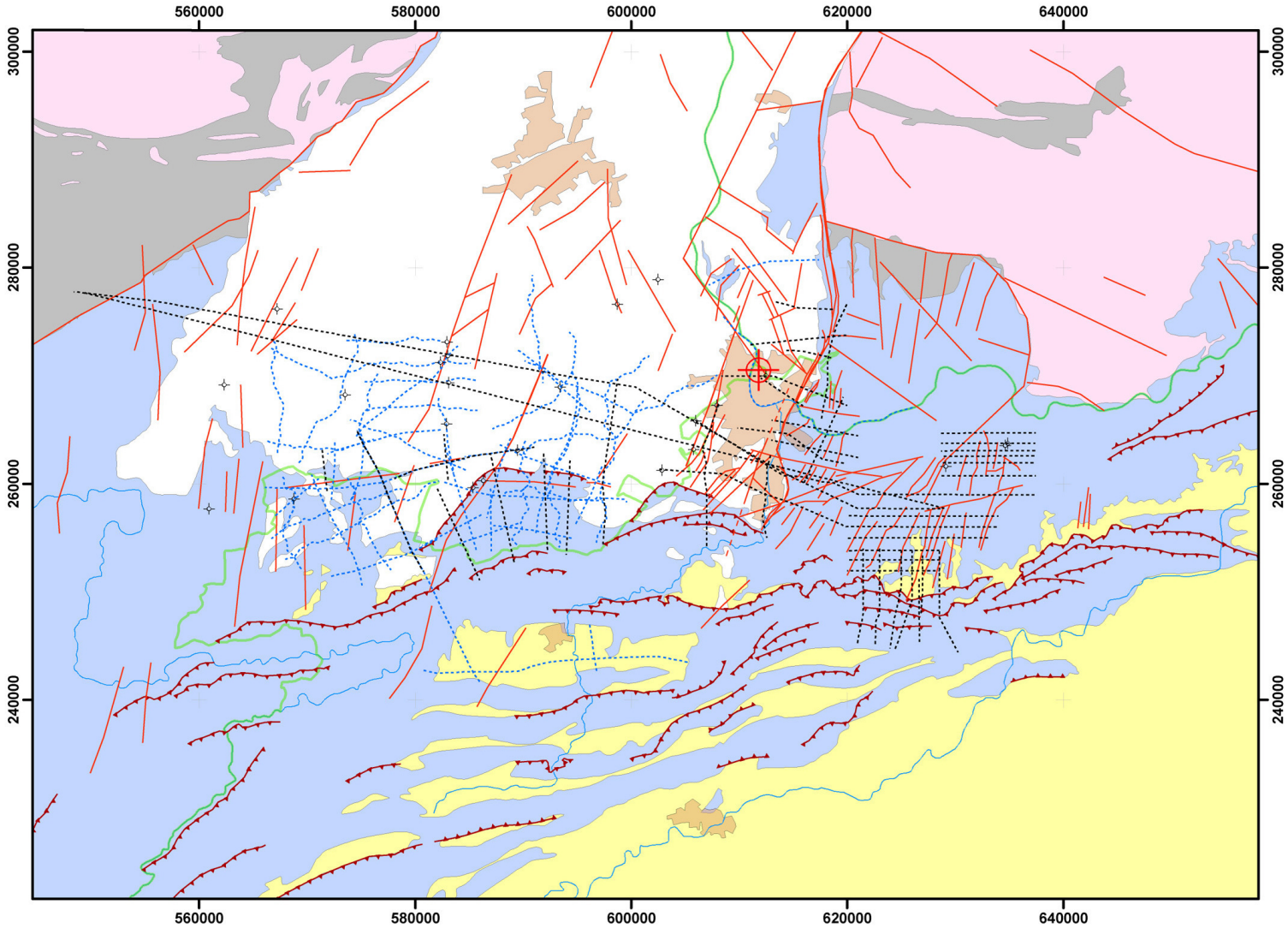

B - Overlap of selected used maps (not exhaustive for visualization purposes), see text for references.

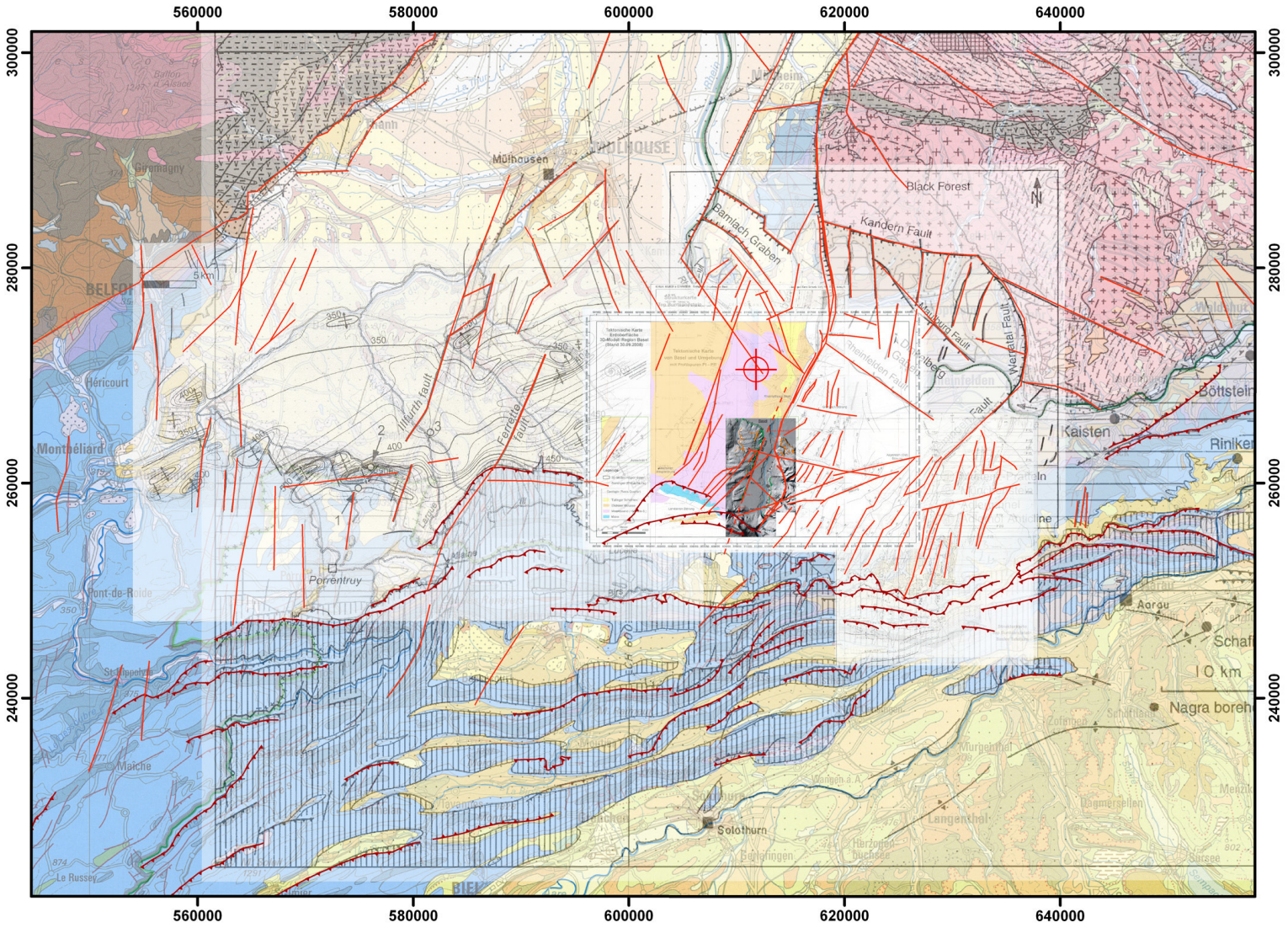

3.1.2 Regional fault families (inheritance and activities)

On the compiled structural map presented in Figure 11, different fault families are shown and can be described by their associated tectonic phase (inheritance):

- Hercynian NW-SE oriented fault family: the Variscan-Hercynian orogen developed from Devonian to Permian times and resulted in a double-verging mountain belt that covers the whole Western Europe (Güldenpfennig & Loeschke 1997; Hann et al. 2000; Vaida et al. 2004; Ziegler & Dèzes 2005; Ziegler & Dèzes 2007). The Upper Rhine Graben transects the internal parts of this orogen, characterized by a south-dipping suture in its northern part (Saxo-Thuringian/Bohemian suture) and a north dipping one in its southern part (Bohemian/Moldanubian suture). By Stephanian-Early Permian times, the disruption of the Variscan orogen was accompanied by widespread alkaline intrusive and extrusive magmatism, similar to the granitic pluton encountered in the Basel1 reservoir. This complex orogenic history gives rise to a well-preserved NW-SE fault family.
- Permo-Carboniferous E-W oriented fault family: the wrenched-induced collapse of the hercynian orogen formed a system of ENE-WSW trending transtensional basins, reactivating the Variscan structural grain mainly by dextral shearing (Ziegler & Dèzes 2005; Ziegler & Dèzes 2007). In the area of Basel, this tectonic phase produced a more E-W trending fault family, by which the transtensional activity resulted in the production of detritic graben basins such as the Burgundy/Constance-Frick trough (following the Montbéliard-Mandach line of Laubscher 2007), separated from the graben underlying Basel (with 764 m of permo-carboniferous sediments in the Basel1 borehole) by a narrow E-W oriented horst located beneath the northern front of the Jura. This fault system was reactivated during later graben opening in a sinistral transtensive mode, while it is supposed to act in a dextral transpressive mode at present times (Ustaszewski 2004 and references therein).
- Rhenish NNE-SSW oriented fault family: the opening of the Upper Rhine Graben followed a period of relative tectonic quiescence during which the area was somewhat affected by the evolving alpine orogen: firstly by Mesozoic subsidence and relative sediment deposition during the opening of the alpine Tethys, and secondly by Paleocene to Mid-Eocene uplift and erosion during the first stages of collision in the Alps and the Pyrenees (Dèzes et al. 2004 and references therein). Rifting initiated in the Upper Eocene under WNW-ENE to W-E extension (Ustaszewski 2004; Larroque & Laurent 1987; Lopes Cardozo & Behrmann 2006), producing NNE-SSW oriented faults, such as the major eastern border fault of the graben (Rhine Valley Flexure fault). By early Neogene times and up to present times, the NW-oriented stress field changed the tectonic setting of the Upper Rhine Graben as a whole shear-oblique sinistral rift system (Ustaszewski 2004; Dèzes et al. 2004; Laubscher 2001).

These inherited fault families, with different orientations, are supposed to behave differently in the current transcurrent stress field characterized by a NW-oriented main compression axis (see section 2.3.1. for details concerning the stress field). While NNE-SSW Rhenish faults appear quite well-oriented for re-activation in a sinistral mode (at 40-50° from S1

direction), E-W Permo-Carboniferous faults should act as dextral transpressional features (at almost 60° from S1) even if it appears mechanically difficult to re-activate such steep faults (with normal geometries dipping at almost 70°) with a compression component. For the NW-SE Hercynian fault family, the orientation from the NE-SW S3 minimum stress axis would cause an extensional re-activation, but the transcurrent nature of the stress field should inactivate these fault orientations. However, as described in section 2.3.1, the occurrence of both strike-slip and extensional earthquakes in the Basel area suggests that extensional movements are possible for these NW-SE faults.

3.1.3 The Basel 1356 earthquake: literature interpretations

The Basel 1356 earthquake, with maximum intensity of IX-X and magnitude estimates between 6.0 and 6.9 (Mayer-Rosa & Cardiot 1979; Fäh et al. 2003; Lambert et al. 2005), plays a major role in our study, as it highlights the general concern of the population of Basel about the regional seismic risk, leading many people to react strongly after the minor events induced by the stimulation of the Basel1 reservoir. Different tectonic interpretations have been proposed to explain this earthquake, pointing to different fault systems (Figure 12):

- sinistral re-activation of the main eastern border fault of the graben (Rhine Valley Flexure Fault, RVF): this fault belong to the NNE Rhenish family and has been proposed as the host of the 1356 event (Laubscher 2007). In the current stress field, it should act as a strike-slip sinistral fault, while some observations point out a possible extensional (at least partly) current activity (geomorphology, Kock 2008).
- dextral transpressional re-activation of E-W Permo-Carboniferous graben border fault: an important horst-and-graben system underlies the Mesozoic cover south of Basel, and is bordered by E-W inherited normal faults that could be re-activated as dextral transpressional structures. Without pointing to a particular fault, this fault trend has also been proposed as responsible for the 1356 earthquake (Ustaszewski 2004; Laubscher 2007; Schmid & Slejko 2009). As noted however in the previous section, their dips seem too steep for a re-activation with a compression deformation component.
- Jura thusting: some authors have analyzed the possibility of a thrusting 1356 event on a fault belonging to the Jura fold-and-thrust belt (Meyer et al. 1994). Evidences have been found for recent compression features at the front of this mountain belt (Pliocene Sundgau gravels folding; Ustaszewski 2004), but they appear linked to the inherited Permo-Carboniferous fault system in a sinistral thick-skin transpressional deformation mode (analog to the previous description of Permo-Carboniferous faults re-activation), while the thin-skinned thrust-related folding of the Jura appears either inactive or aseismic (thanks to ductile shearing in evaporite decollement layers).
- Basel-Reinach fault: palaeoseismological investigations along the 8 km long Basel-Reinach geomorphologic scarp have lead to the observation of a fault affecting Quaternary deposits, trenched in several sites (Ferry 2004; Ferry et al. 2005; Meghraoui et al. 2001). This fault shows evidence of normal movement, with colluvial wedge deposits supposed to date different seismic events. One of these events happened between AD500 and AD1450, thus matching the 1356 earthquake's time

frame. This fault has therefore been proposed as a candidate for hosting the 1356 event, while the dating of other wedge deposits lead to proposing recurrence times and associated fault dynamics (see section 2.3). Despite these detailed studies, this interpretation is much debated (*e.g.* Laubscher 2007; Schmid & Slejko 2009): some believe that geomorphologic features do not match the theory (Birse river flowing on the “wrong” side of the valley) or argue that the fault should be regarded as a gravitational slide (nevertheless, sliding events could also be indirectly linked to regional seismicity). The NNE orientation of the Basel-Reinach fault (if this is a fault) would imply sinistral strike-slip movements in the current stress field, while it is interpreted as a pure extensional feature by the authors. Another view combines these two proposals with oblique slip transtensional movements, but this explanation would then imply unrealistic slip rates (see section 2.3).

Without a reliable consensus regarding the fault that was activated during the 1356 event, we considered all hypotheses as working cases to analyze the possible activity of the faults of our models.

Figure 11: Large-scale view of our structural model with seismotectonic data

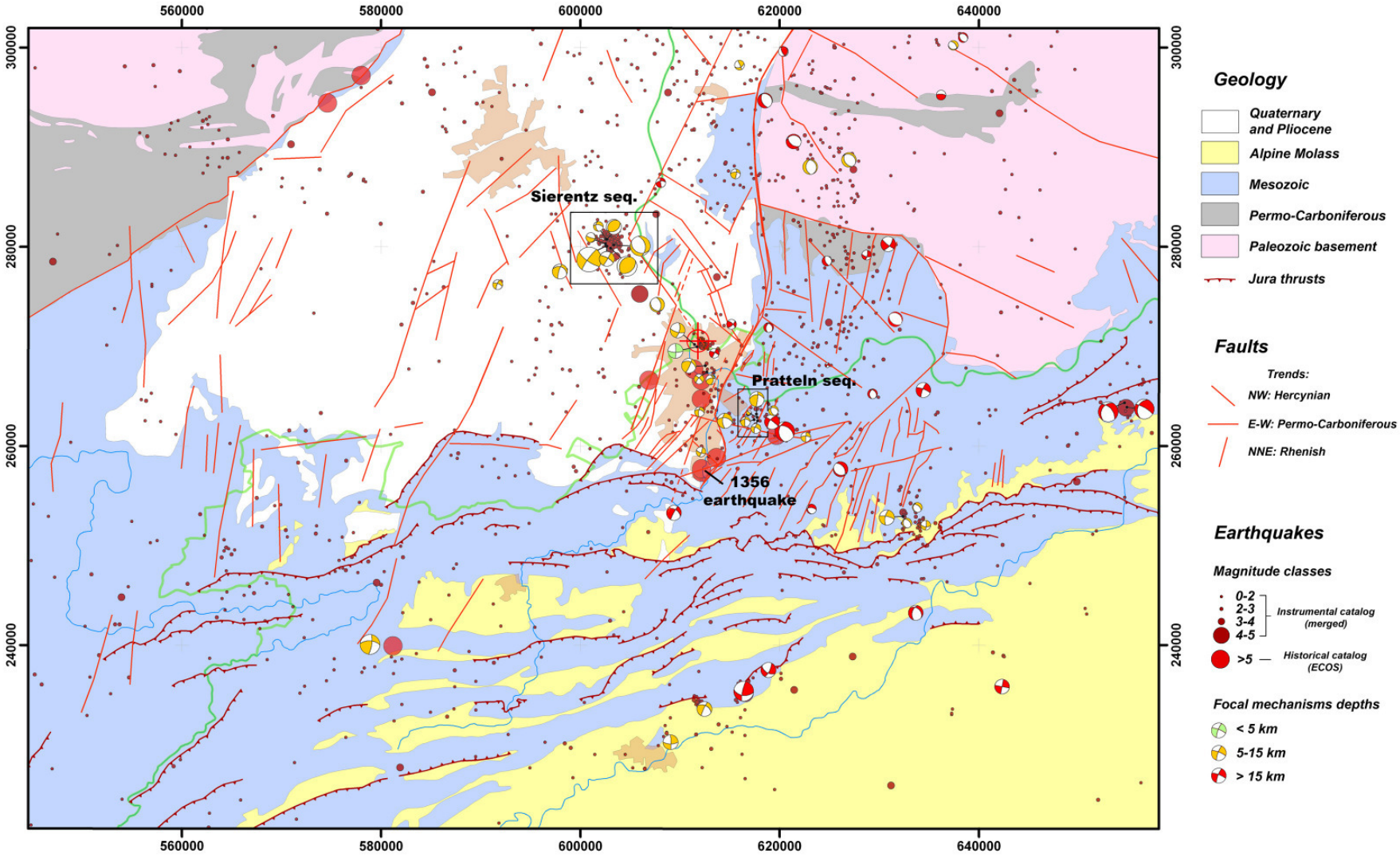

Figure 12: Fault model in the region of interest

A: surface map, B: horizontal section at 5 km depth (surface geology for indication, hatched polygons representing fault location uncertainties at depth).

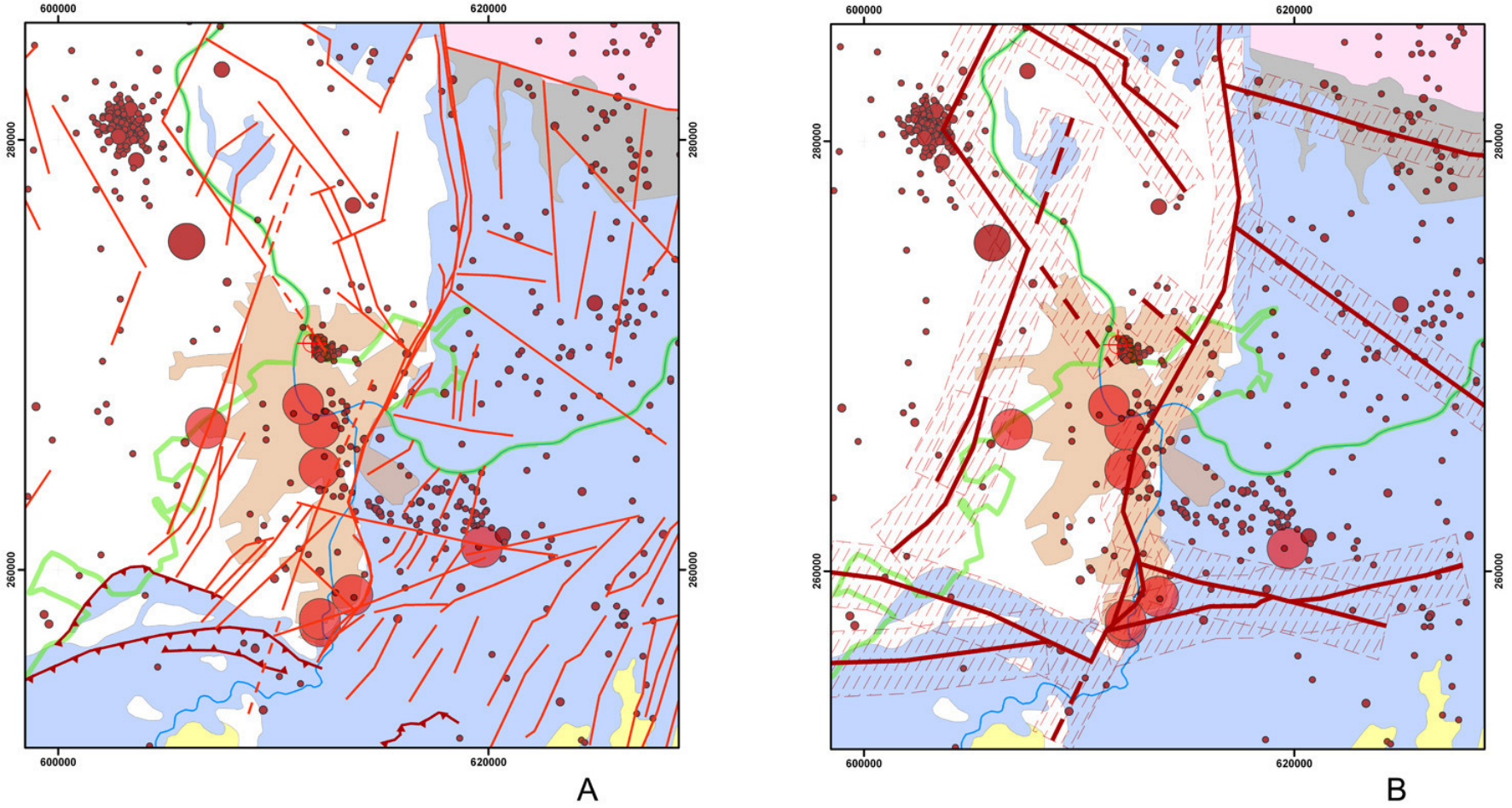

3.2 Fault model

Our fault model is presented in Figure 11. It covers the whole Southern Rhine Graben, and more specifically an area that spreads over a few tens of kilometers around the borehole, resulting in an artificially denser fault pattern in this region. To analyze the fault pattern at depth and the relationship with regional seismicity, a horizontal map of fault traces at 5 km depth (the depth of the reservoir) was drawn (Figure 12).

3.2.1 Fault pattern – relationship with regional seismicity

The Basel area is located at the southeastern corner of the Southern Rhine Graben, and is surrounded by a system of NNE oriented Rhenish faults to the east (Rhine Valley Flexure RVF: main eastern graben border fault) and west (Alschwill fault), while it is bordered to the south by the last outer Jura fold, the location of which corresponds to a deeper WNW-ESE Permo-Carboniferous fault beneath the Mesozoic cover. North of Basel, NW oriented faults dissect the graben filling in an oblique NW-SE horst and graben system, re-activating older Hercynian structures.

More to the west, the fault pattern becomes less dense because of the Quaternary graben sedimentary filling, less fractured than the outcropping Mesozoic units east of the RVF (Dinkelberg Block) that present a dense network of small (5-10 km long) faults, unroofing in the Triassic decollement horizon and not affecting the crystalline basement (Huggenberger & Dresmann 2009; Spottke et al. 2005; Bonjer 1997). A few inherited faults are however also supposed to affect the basement in this area: they are represented by NW Hercynian faults (such as the Rheinfelden fault) and E-W Permo-Carboniferous faults (Aspenrain fault for example).

To analyze the possible relationship between the fault pattern and the regional seismicity, a complete seismic catalog was computed (see section 2.1 for details on the merging technique) and is represented in Figure 11 and Figure 12. However, as in most cases in seismotectonics, the identification of seismic events related to a particular known fault appears very difficult to achieve. Indeed, given the location uncertainties of earthquakes (a few kilometers) and also of faults at depth, one can hardly assign a fault to an event. Even if one can argue that all earthquakes represent a slip on a fault, it appears that every new seismic event (or sequence) reveals new fault patches that are in most cases different from the fault network mapped at the surface. This is particularly the case in the Pratteln seismic sequence (southeast of Basel), where a seismic sequence had revealed N-S sinistral activated faults (by high-precision relative location techniques; Deichmann & Garcia-Fernandez 1992; Kastrup 2004) whereas the major fault mapped at the surface is E-W oriented (Aspenrain fault), so the relationship between this fault and the earthquakes of the sequence is (at best) only indirect.

Nevertheless, a possible relationship between seismicity and mapped faults was found in the Sierentz seismic sequence northwest of Basel. This sequence, concentrated at 10-12 km depth, appears complex, with a mix of extensional, transcurrent and even compressional events (see focal mechanisms, Figure 11) and presents a general alignment of events oriented NW-SE, particularly similar in strike to the nearby Sierentz fault. When prolonged at

depth, this fault appears very close to the seismic sequence (considering location uncertainties of both events and fault), with the main events concentrated at its northwestern end, where it joins a NNE oriented Rhenish fault. This particular location, at the junction between two faults, could explain the complex nature of deformation regimes seen from focal mechanisms, with compressional mechanisms compatible with faulting on NE oriented structures and extensional ones with faulting on NW oriented structures. Even though a close relationship with the Sierentz fault cannot be proven satisfactorily, at least an indirect link can be suggested, and this fault geometry at depth could be better understood by an extension right to the seismic sequence (by assigning a dip of 84° to the fault). Moreover, this seismicity/fault relationship could be used to assign a current activity to the Sierentz fault, which would also be compatible with the observation of quaternary faulting on a nearby similar fault (Kock 2008).

Although an apparent NW-SE large-scale alignment of earthquakes (almost 40 km long) appears at first glance from Sierentz to Zeglingen (Sissach district), the exact nature of this lineament is questionable (Figure 11). Referred to as the Adlerhof line (Laubscher 2007), this striking trend line appears as a region of concentrated seismicity, without any direct link to known geological structures, so that we don't interpret it as the expression of seismicity following a fault or a fault zone, but more to a region of weakness that concentrated the deformation (although a possible artifact of visualization is also possible by the apparent alignment of the Sierentz, Pratteln and Zeglingen sequences). Consequently, no fault following this alignment has been constructed in our model.

3.2.2 Selection of relevant faults for the risk analysis (confidence levels)

A qualitative selection of relevant faults for the risk analysis was completed on the basis of proximity to the borehole, fault activity and regional importance. Selected faults are presented in Figure 13 and Table 3 together with data sources and associated confidence levels, related to uncertainties assigned to the used database. For each fault, the confidence rating for surface mapping of faults was considered higher than for depth positioning, given the large uncertainties of fault depth interpretation. Some major faults appear well-resolved by surface or sub-surface mapping techniques (geological investigation or reflection seismics), as they correspond to major geological regional limits (RVF for example), whereas other faults appear to be more speculative, hence inheriting a lower confidence level (Weil-am-Rhein fault for example).

The major Rhine Valley Flexure fault (RVF) has a complex configuration, bordering the whole eastern limit of the graben in a more or less continuous manner. Nevertheless, it seems unrealistic to imagine a continuous fault extending over the whole mapped area, so instead we propose an array of fault patches (based on literature interpretations; Gürler et al. 1987; Huggenberger & Dresmann 2009) that follow the main fault zone, with different persistencies and confidence levels (Figure 13, Table 3). Additionally, some faults may extend into areas that are not covered by any observation. This is the case for the Sierentz and Alschwill faults, which are prolonged to the southeast and northeast, respectively. This is also the case for the Basel-Reinach fault that has been extended by 5km into northern and southern directions to make it large enough for hosting an M6.5 earthquake. The surface expression of this fault as proposed in Ferry et al. (2005) does not indicate a fault area large enough for an M6.5

earthquake; however, continuations of the fault to the north (below Basel) and inside the Jura to the south are suggested by different authors (Ferry 2004, Huggenberger 2009, Laubscher 2007, Schmid *pers. comm.*). The selected Permo-Carboniferous graben border fault, to the south of Basel, is special as it only appears at a depth of about 500 m (beneath the Mesozoic cover) and then is only represented in the 5 km depth map (Figure 13).

These selected faults were computed in 3D by first using the most reliable data to determine all surface points (or sub-surface points in the case of the Permo-Carboniferous border fault), and then modifying the dip of the faults in order to adjust to the various possible interpretations at depth (see Table 3). Because of the highly speculative nature of deep fault curvature interpretations (listric shapes) (*e.g.* Ustaszewski 2004), we decided to stick to linear representations of fault planes at depth (straight lines cross-sections), while surface fault traces display more complicated patterns, matching known fault exposures.

Although it was not possible to directly associate hypocenters from the merged catalogue to the faults derived in the current study, we used the hypocentral depth of the seismic activity occurring in the vicinity of the faults as an indicator of vertical fault extension. While one can not rule out the possibility of a prolongation of faults down to the base of the seismogenic crust (maximum depth of regional seismicity: 30km), from this analysis we obtain:

- Sierentz fault: extension until 14 km depth,
- Alschwill fault: until 14 km depth,
- Rhine Valley Flexure fault: until 25 km depth,
- Weil-am-Rhein fault: until 25 km depth,
- Basel-Reinach fault: until 16 km depth,
- Aspenrain fault: until 22 km depth,
- Rheinfelden fault: until 25 km depth,
- Permo-Carboniferous border fault: until 20 km depth.

Figure 13 shows a set of 8 faults that we consider to be relevant for the current risk study. Their dimensions makes these faults prone to host large magnitude earthquakes (M>5), while their proximity to the Basel 1 borehole points to a possible modification of their seismic cycle by geothermal exploitation (AP4000 contribution), so we did not consider more distant faults.

Figure 13: Selected faults for the risk analysis
(see Table 3).

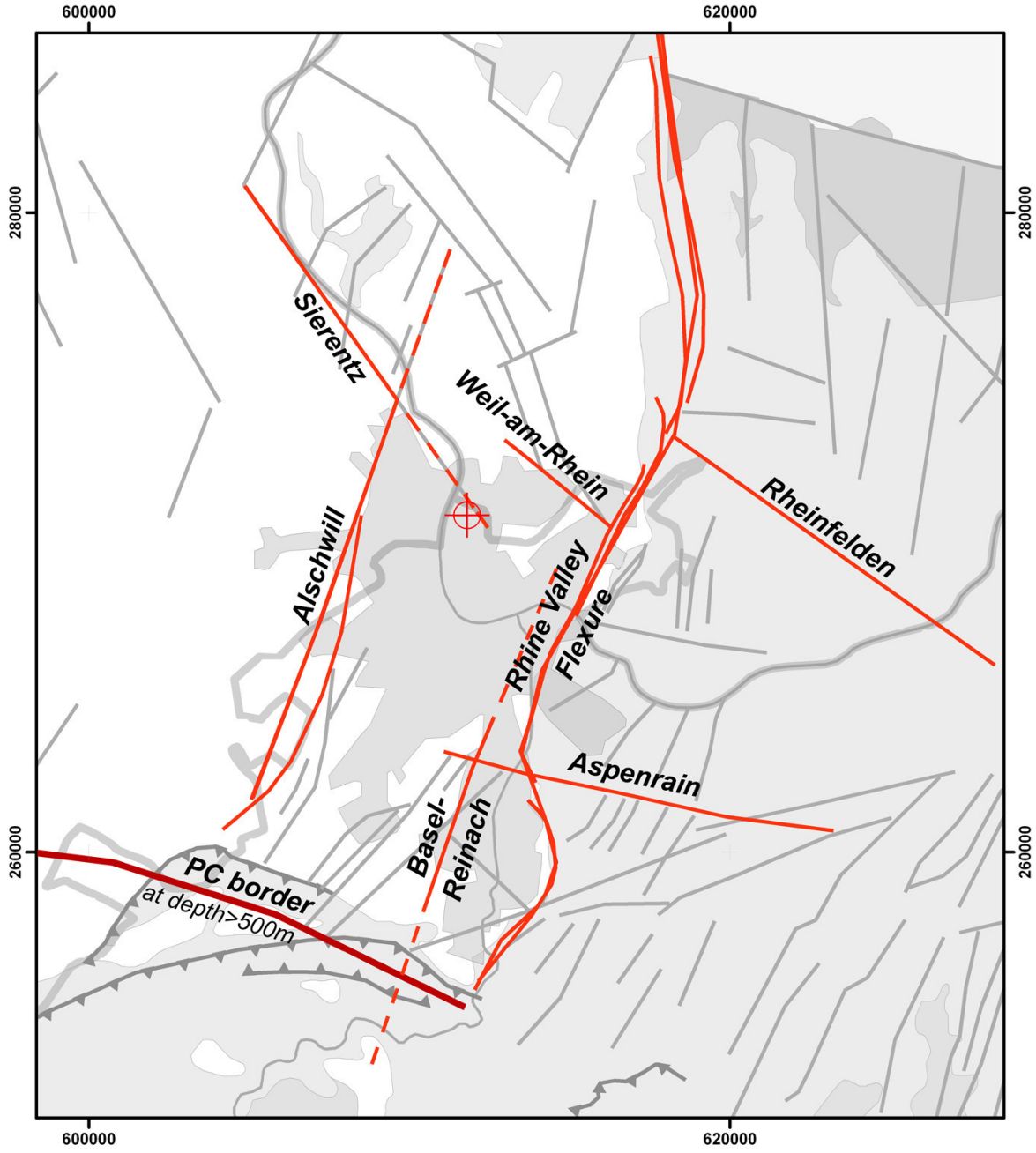

3.3 Fault dynamics

By “fault dynamics”, we mean all parameters that control the faults activity in terms of stress and strain, and more specifically the quantification of the stress field and of slip rates (and recurrence times) affecting the faults. These parameters play an important role in the modeling study of AP4000, so that a particular chapter of this report is dedicated to this analysis. As presented below, some direct investigations were carried out to estimate these parameters (borehole data or specific fault analyses), but they appear too punctual and

uncertain (large range of possible values) to make a direct estimation assigning specific parameters to each fault of the model. Consequently, we decided to propose more general/regional considerations, with uncertainty estimations, and then we will export a range of possible values that will be tested by AP4000 modeling studies.

3.3.1 Stress field

The orientation of the stress field is well-defined by both focal mechanism data (inside the reservoir or regionally) and borehole induced fractures analysis. Induced earthquakes show typical strike-slip mechanisms, with two normal faulting events and a few intermediate mechanisms (see chapter 1). The orientation of T-axes (the most stable measure of the horizontal component of deformation) for these induced events appears close to T-axes orientations of natural regional focal mechanisms (differing by less than 15-20°), placing the extensional axis in a NE orientation (N-46 ± 11° for induced events, N-63 ± 16 for natural ones ; Deichmann & Giardini 2009). Moreover, stress inversion of regional natural events gives an orientation of the minimum principal stress S3 of about N-54° (Kastrup et al. 2004; Delacou et al. 2004), thus compatible with induced focal mechanisms, orientation differences cannot be considered as a significant evidence for an anomalous behavior caused by water injection. Stress inversion also gives a N-141° to N-147° orientation of the maximum principal stress direction S1 (Kastrup et al. 2004; Delacou et al. 2004).

The analysis of more than 9,000 borehole induced fractures (Valley & Evans 2009; Evans & Roth 1998) also gives estimations of the maximum horizontal stress axis SHmax, with a mean orientation of N-151 ± 13° from DITFs (Drilling Induced Fractures) and N-143 ± 14° for borehole breakouts. The combined value weighted for frequency of occurrence being N-144 ± 14°, this appears highly similar to the results of focal mechanisms studies presented above. No marked dependence with depth was observed in the granite for the drilling induced derived estimations of stress directions, so that one can consider these orientations as relatively stable in basement rocks, whereas it appears more erratic in the sedimentary cover (Valley & Evans 2009 and references therein), probably because of the influence of topographic/gravitational effects or sedimentary layering. Moreover, the compatibility with both local and regional focal mechanisms estimations allows us to propose orientation values relevant for both local and regional studies, which are **N-54° for S3** and **N-144° for S1**. The main regime being in the strike-slip mode of deformation, these stresses can be considered as sub-horizontal (dip 0°). Nevertheless, one cannot exclude some possible local variations of stress directions, especially near major regional faults that could significantly deviate the stresses, but without any concrete data supporting this hypothesis, the given values should be considered as relevant for our study.

Quantifications of stresses were performed by Häring et al. 2008 who in the first place modeled the magnitudes of horizontal and vertical stresses in the Basel1 borehole (Figure 14). The vertical stress Sv, which represents the overburden, was calculated by integration of the density log, while horizontal stresses were estimated by software modeling calculation (see Häring et al. 2008 for more details). Moreover, a lower bound constraint on the magnitude of Shmin is provided by the hydraulic stimulation data, where no pressure-limiting behavior was observed, thus indicating that the maximum injection pressure (74 MPa downhole pressure) did not exceed the magnitude of Shmin. Also, an upper bound on the

magnitude of SHmax is provided by using the concept of in situ stress limitations from the frictional strength of faults. Assigning a range of 0.6 to 1 to the frictional coefficient μ yields estimates ranging from 160 to 255 MPa for Shmax at 5 km depth. Without any other magnitude estimation of stresses in the Basel area, these data must be considered as the most relevant ones that should be used in the modeling study of AP4000, although some variation (local or regional) cannot be excluded, especially considering the unreliability of magnitude estimates.

Figure 14: Stress field quantifications in Basel1 borehole (Häring et al. 2008)

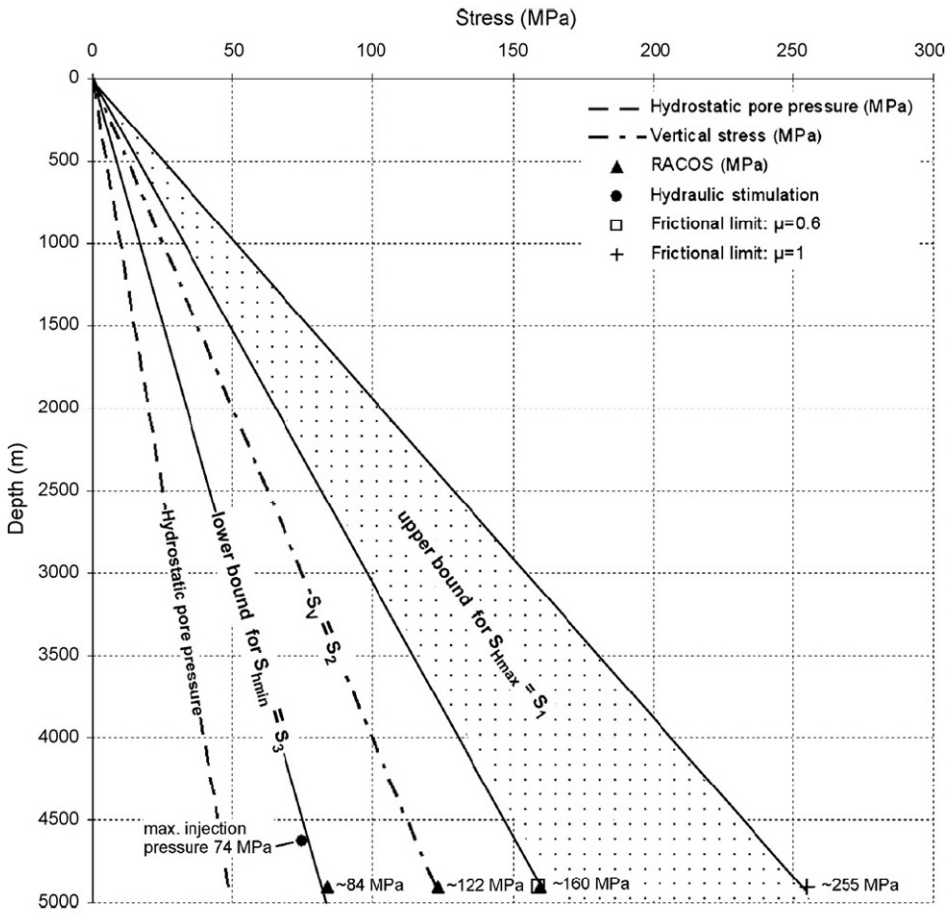

3.3.2 Recurrence – slip rates: Basel-Reinach model

Given the low speed of crustal block motions observed in most West European areas (< 1 mm/y), estimations of strain rates affecting faults appear as a particular difficult task to deal with. In the Basel area, one case study has been fully described, and corresponds to the Basel-Reinach fault (see also section 2.1), which was earmarked as responsible for the great Basel 1356 earthquake (Meghraoui et al. 2001).

Palaeoseismological trenching studies on this fault (Ferry 2004; Ferry et al. 2005;) revealed repeated colluvial wedge deposits, supposed to date different major seismic events on the fault. The dating of these deposits provides estimations of recurrence periods for earthquakes comparable to the 1356 event. This study resulted in the identification of 5

major earthquakes in almost 10,000 years (see Ferry 2004 for more details), with magnitude estimations ranging from Mw 6.3 to 6.7, and corresponding to an average recurrence period of **2300 to 2600 y**.

Moreover, the measuring of fault offsets in colluvial wedges gives average values of uplift rates of about **0.27 mm/y**, corresponding to slip rates of about 0.29 mm/y in the dip slip direction (extension mode), and to almost 0.32 mm/y if one considers a transtensional oblique slip direction (personal estimation) with an extension axis parallel to the S3 stress axis. In this case, the horizontal component of strike-slip motion would attain almost 0.15 mm/y. These displacements are not discussed by Ferry et al. 2005, because they only consider the normal components of movements on the fault (since the trenches are perpendicular to the fault, it is almost impossible to observe horizontal movements). The orientation in the stress field would imply a sinistral (with a slight transtensional component) deformation on this N-20 oriented fault.

Other estimations of uplift rates affecting the Basel-Reinach fault come from geomorphologic (Birse river terrace offsets across the fault) and geophysical (seismic and electrical profiles) studies, and yield comparable values -for both analyses- of about **0.1 mm/y**.

As discussed in section 2.1, this Basel-Reinach fault study is highly controversial, some authors believing that it reflects gravitational sliding events instead of direct seismic events, or that the Basel-Reinach scarp could be related to sedimentary compaction effects on the borders of the Birse valley. Whatever the exact nature of the scarp (seismic fault or indirect faulting or sliding events), the dating of colluvial wedges (or indirect slided deposits) could reflect the occurrence of large regional seismic events, such as the 1356 one, thus providing indirect estimations of recurrence periods of such events.

3.3.3 Recurrence – slip rates: other estimations

Other more or less direct estimations of fault dynamic parameters can be carried out in the Basel area to better constrain the range of possible values.

For recurrence times, one can refer to the statistical Guttenberg-Richter relationship, which yields estimates ranging from 40 y for a Mw 4 event to 9,000 y for a Mw 7 one (a-value: 2.31, b-value: 0.9, corresponding to the highest weighted values for the Basel area in the Seismic Hazard Assessment of Switzerland report of Giardini et al. 2004). More specific values can also be proposed by considering the range of fault areas (km^2) for the selected relevant faults exported to AP4000, which provides empirical estimates of maximum magnitude earthquakes than could happen on each fault (by using the log-linear relationship of Wells & Coppersmith 1994). These estimates can then be in turn converted into recurrence periods using the Guttenberg-Richter relationship. Areas ranging from 25 to 800 km^2 yield estimates of magnitudes ranging from 5.4 to 6.9, corresponding to recurrence intervals between **400 and 8,000 y**. The range remains wide, but no other estimations (except the Basel-Reinach case) can be achieved to restrict it.

For what concerns the slip rates affecting the faults, estimations other than the Basel-Reinach case study provide interesting data. The study of Rhine river terraces, for example,

shows a possible progressive tilting of previously supposed sub-horizontal levels, and gives estimates of vertical movements of about 0.05 mm/y (Kock 2008), even though the authors point out the large uncertainty associated with their estimation. High precision seismic profiles are also available for the whole Rhine river from Mannheim to Rheinfelden, and propose estimations of vertical slip rates affecting faults, based on fault offset measurements of the base Quaternary horizon (Bertrand et al. 2006). Cumulated offsets of 7.1 to 61.7 m yield vertical slip rates ranging from 0.0039 to 0.0343 mm/y (considering an age of 1.8 Ma for the base Quaternary). However, the authors do not point to any particular fault, so that these estimates are only useful as regional constraint values. Also, the authors do not discard the possibility of a strike-slip component along some faults, as clear flower structures were observed in some places (not quantified). Other structural considerations come from finite displacements observed on faults from literature cross-sections, combined with an estimation of movement persistence along faults. Fault offsets ranging from 100 to 2,000 m (for selected relevant faults) with a persistence of 7 to 35 Ma (main extensional Oligocene phase only or total graben formation duration until present) result in this case in estimations ranging from 0.003 to 0.29 mm/y.

The overall extension of the Southern Rhine Graben has been estimated by restorating the top Mesozoic horizon (Ustaszewski 2004) and appears quite low with 5.3% extension for the total rift transect. By applying this extension to 5 to 15 major faults across the graben, and using a phase duration of 7 Ma (proposed value of Ustaszewski 2004, that is the Oligocene extension phase), estimates of slip rates range from 0.04 to 0.13 mm/y.

Other estimations, mostly relevant to understand current fault activity, come from GPS measurements. The work of Tesauro et al. 2005 reveals 2.10^{-9} y^{-1} of shortening strain rates (in the NW orientation) in the Basel area, which leads to qualitative assessments of slip rates ranging from 0.01 to 0.03 mm/y by considering the total strain acting on 5 to 15 faults across an 80 km section crossing the overall southern graben. The same calculation applied to the data of Delacou et al. 2008, which gives maximum GPS-based extensional strain rates of 2 to 3 10^{-8} y^{-1} (not well-constrained but used to position upper bounds), yield slip rates ranging from 0.11 to 0.48 mm/y. Both shortening and extensional deformation are compatible with a strike-slip deformation regime, where both the extension in the S3 direction and the shortening in the S1 direction are competing in a subtle manner on the fault pattern to produce overall NE extension and NW compression of the graben. In the same way, the folding of Pliocene Sundgau gravels at the northern front of the Jura belt corresponds to 0.05 mm/y of post-Pliocene shortening (Ustaszewski 2004), a value that is comparable to the extensional rates presented above.

Globally, overall slip rate values range from 0.003 to 0.5 mm/y, while a more realistic range can be proposed based on GPS calculations and fault offsets (the most relevant data according to us), with values from **0.03 to 0.3 mm/y**.

Table 3: Selected relevant faults

Rhine valley Flexure

Azimuth : N-NNE
Dip : 70° (to W) ±10
Length (m): 5 000 - 50 000 (branches)
Activity in the regional stress field: SS left-lateral
Max. depth (m): 25 000 (max. 30 000)

Data source	Results	Method	Confidence
Gurler et al., 1987	Detailed mapping	Geological sections (from seismics)	80-90 %
Huggenberger	3D model (GoCAD)	Synthesis (geology, geophysics…)	80-90 %
Nagra Tectonic Map (Thury et al.1994)	Structural map	Synthesis (geology, geophysics…)	70-80 %
Ustaszewski (thesis, 2004)	Deep cross-section (Moho)	Synthesis	15 % (on depth interpretation)
Koch (thesis, 2008)	Pleistocene activity	Geomorphology (river terraces)	15 % (on fault activity)

Activity
Neotectonic indices from the tilting of Rhine river terraces (Koch, 2008) - 0.05 mm/y

Remarks
Main eastern border fault of the southern Rhine graben

Sierentz

Azimuth: NW
Dip: 83° (to SW) ±15
Length (m): 8 - 13 000
Activity in the regional stress field: Normal
Max. depth (m): 14 000 (max. 30 000)

Data source	Results	Method	Confidence
Nagra Tectonic Map (Thury et al.1994)	Structural map	Synthesis (geology, geophysics…)	70-80 %
Koch (thesis, 2008)	Pleistocene activity	Geomorphology (river terraces)	15 % (on fault activity)
Bertrand, 2006	Quaternary activity (this fault?) 0.0039 – 0.0343 mm/y	High resolution river Rhine seismics	30-50 % (on fault activity)

Activity
Possible link with Sierenz seismic sequence, associated fault with field evidence of Quaternary activity (NW-SE fault at SW) - Kock 2008 + Quaternary offsets (Rhine seismics)

Remarks
Relationship (direct?) with the Sierentz seismic sequence (~10-12km depth) - dip constrains (83°)
Prolongates to the SE into the reservoir but could stop on the Alschwill fault (Nagra Tectonic Map)

Alschwill

Azimuth: NNE
Dip: 70° (to W) ±15
Length (m): 11 - 18 000 (2 branches)
Activity in the regional stress field: SS left-lateral
Max. depth (m): 14 000 (max. 30 000)

Data source	Results	Method	Confidence
Gurler et al., 1987	Detailed mapping	Geological sections (from seismics)	80-90 %
Huggenberger	3D model (GoCAD)	Synthesis (geology, geophysics…)	80-90 %
Ustaszewski (thesis, 2004)	Deep cross-section (Moho)	Synthesis	15% (on depth interpretation)
Kock (thesis, 2008)	Pleistocene activity (north prolongated)	Geomorphology	15 % (on fault activity)

Activity
Unknown

Remarks
Doubtful from Geothermal Explorer (based on drilling infos)

Basel-Reinach

Azimuth: NE
Dip: 70° (to W) ±10
Length (m): 6 500 - 16 500 (branches)
Activity in the regional stress field: SS left-lateral
Max. depth (m): 16 000 (max. 30 000)

Data source	Results	Method	Confidence
Ferry (thesis, 2004)	Neoteconic-historical activity 100 ±20 m total offset 2300-2600a reccurrence (1356-type earthquake) 0.1-0.27mm/y (Pleisto – Holocene slip rates)	Palaeoseismological investigations (trenching, geophysics, geomprohology)	40-60 %
Gurler et al., 1987	Detailed mapping (inverse dip at depth from Ferry)	Geological sections (from seismics)	80-90 %
Huggenberger	3D model (GoCAD)	Synthesis (geology, geophysics…)	80-90 %

Activity
Neotectonic indices: palaeoseismological evidences (contested)…

Remarks
Proposed fault for the 1356 earthquake
Discussions on the possible gravitational origin of the Reinach scarp of Ferry…
The Birse river should flow on the western (scarp) side of the valley - geomorphological contradiction
Field evidences (electrical profiles) on the existence of the fault (relevant for Huggenberger)
Discussions on the horizontal component of movement (in the known stress-field, this fault should act as left-lateral)
Link to the Rhine valley flexure fault at depth?

PC border fault

Azimuth: WNW-ESE
Dip: 70° (to N) ±15
Length (m): 26 000
Activity in the regional stress field: SS right-lateral (reverse component)
Max. depth (m): 20 000 (max. 30 000)

Data source	Results	Method	Confidence
Ustaszewski (thesis 2004) and references therein	Map of PC deposits	Synthesis (geology, geophysics…)	40-50 %

Activity
Indirect neotectonic indices: Sundgau gravels (Pliocene) folding - 0.05 mm/y (shortening) - Ustaszewski 2004

Remarks
Highly interpretative (fault interpretation), thicknesses of PC from wells and seismics, narrow horst at the northern border of Jura folds bounded by normal faults

Weil am Rhein

Azimuth: NW
Dip: 75° (to SW) ±20
Length (m): 4 300
Activity in the regional stress field: Normal
Max. depth (m): 25 000 (max. 30 000)

Data source	Results	Method	Confidence
Gurler, 1987	Detailled mapping	Geological sections (from seismics)	50-60 %
Huggenberger	3D model (GoCAD)	Synthesis (geology, geophysics…)	50-60 %

Activity
Unknown

Remarks
Very few infos on this structure…

Aspenrain

Azimuth: E-W
Dip: 70° (to S) ±10
Length (m): 17 000
Activity in the regional stress field: SS right-lateral
Max. depth (m): 22 000 (max. 30 000)

Data source	Results	Method	Confidence
Huggenberger (+Spottke, 2005)	3D model (GoCAD)	Synthesis (geology, geophysics…)	80-90 %
Gurler et al., 1987	Detailed mapping	Geological sections (from seismics)	80-90 %

Activity
Current activity unknown, offsetting mesozoïc sediments

Remarks
Relationship (direct?) with the Pratteln seismic sequence? (but left-lateral clusters imaged on N-S fault…)
Thrusting component (linked to the Adlerhof anticline?) supposed for Eocene-Oligocene activity. No evidence of younger movements - Ref Spottke et al. 2005

Rheinfelden

Azimuth: NW-SE
Dip: 70° (to NE) ±10
Length (m): 12 000
Activity in the regional stress field: Normal
Max. depth (m): 25 000 (max. 30 000)

Data source	Results	Method	Confidence
Nagra Tectonic Map (Thury et al. 1994)	Structural map	Synthesis (geology, geophysics…)	70-80 %
Huggenberger (+Spottke, 2005)	3D model (GoCAD)	Synthesis (geology, geophysics…)	80-90 %

Activity
Unknown

Remarks
Hercynian inherited fault

4 CONCLUSIONS

The present AP2000 contribution corresponds to the first step of the SERIANEX study, which aims at assessing the seismic risk associated to the exploitation of the Basel deep enhanced geothermal system. This present report proposes fault models that will be used by the following work packages to estimate the seismic hazard. It results in:

- a local fault model dedicated to the study of directly induced seismicity, resulting in 8 conceptual faults (or alignments of earthquakes interpreted as faults) within the reservoir, with fault sizes ranging from about 0.05 to 1.15 km^2,
- a regional model in the Basel area, synthesizing the current knowledge of regional potentially seismogenic faults, aiming at the study of indirectly triggered seismicity. 8 faults were selected as relevant structures for the risk study, based on their geographical position and potential activity. No objective reason (fault offsets or seismicity concentration for example) was found to justify faults where no structure is yet mapped, so that no hidden/unknown fault is proposed, although some fault prolongations are suggested in regions not covered by data.

These interpretative geometrical fault models are completed by a study of fault dynamics, to estimate the stress/strain states affecting the faults:

- the stress field is supposed to be homogeneous over the studied area (identical for local and regional studies) with a strike-slip regime characterized by a sub-horizontal NW-oriented maximum principal stress axis (S1 oriented N-144°) and a sub-horizontal NE-oriented minimum principal stress axis (S3 oriented N-54°). The stress magnitude estimates of Häring et al. 2008 are considered to be the most relevant, with quantifications of principal stresses at depth corresponding to 84 MPa for Shmin (S3), 122 MPa for S2 and between 160 and 255 MPa for SHmax (S1) at 5 km depth,
- fault slip rates are hardly documented in the area, and accordingly we do not propose estimations for individual faults in our model. One full-documented case study, the Basel-Reinach fault of Ferry 2004, gives estimations ranging from 0.1 to 0.27 mm/y, while other more or less indirect considerations (see section 2.3.3) refer to a global range of slip rates from 0.003 to 0.5 mm/y. A more precise realistic range is proposed from the analysis of GPS measurements and fault offsets, ranging from 0.03 to 0.3 mm/y.

While the local reservoir model is considered to be well-resolved within the seismically activated zones, no data in the surrounding area establishes the presence or absence of faults, so that a possible direct connection between local reservoir faults and regional ones cannot be excluded (Sierentz fault particularly, see section 2.2.3), thus providing a possible explanation for the loss of water after the shut-in of the well.

Bibliography

Asanuma H., Kumano Y., Moriya H., Niitsuma H., Schanz U., Häring M.O. (2008). Identification of microseismic multiplets in the frequency domain and interpretation of reservoir structure at Basel, Switzerland. *S.E.G. 2008 Annual Meeting*, Las Vegas.

Baisch S., Ceranna L., Harjes H. P. (2008). Earthquake cluster: what can we learn from waveform similarity? *Bull. Seism. Soc. Am.*, vol.98, No.6, p.2806-2814.

Bertrand G., Elsass P., Wirsing G., Luz A. (2006). Quaternary faulting in the Upper Rhine Graben revealed by high-resolution multi-channel reflection seismic. *C. R. Geoscience*, vol.338, p.574-580.

Bonjer K.P. (1997). Seismicity pattern and style of seismic faulting at the eastern borderfault of the southern Rhine Graben. *Tectonophysics*, vol.275, p.41-69.

Bourgeois O., Ford M., Diraison M., Le Carlier de Veslud C., Gerbault M., Pik R., Ruby N., Bonnet S. (2007). Separation of rifting and lithospheric folding signatures in the NW-Alpine foreland. *Int. J. Earth Sci.*, vol.96, p.1003-1031.

Cloetingh S., Cornu T., Ziegler P.A., Beekman F. (2006). Neotectonics and intraplate continental topography of the northern Alpine Foreland. Environmental Tectonics (ENTEC) Working Group. *Earth Science Review*, vol.74, p.127-196.

Deichmann N., Ernst J. (2009). Focal mechanisms of the induced seismicity in 2006 and 2007 below Basel (Switzerland). *Swiss J. Geosci.*, in press.

Deichmann N., Giardini D. (2009). Earthquakes induced by the stimulation of an enhanced geothermal system below Basel (Switzerland). *Seism. Res. Letters*, in press.

Delacou B., Sue C., Nocquet J.M., Champagnac J.D., Allanic C., Burkhard M. (2008). Quantification of strain rate in the Western Alps using geodesy – comparisons with seismotectonics. *Swiss J. Geosci.*, DOI 10.1007/s00015-008-1271-3.

Delacou B., Sue C., Champagnac J.D., Burkhard M. (2004). Present-day geodynamics in the bend of the western and central Alps as constrained by earthquake analysis. *Geophys. J. Int.*, vol.158, p.753-774.

Dèzes P., Schmid S.M., Ziegler P.A. (2004). Evolution of the European Cenozoic Rift System: interaction of the Alpine and Pyrenean orogens with their foreland lithosphere. *Tectonophysics*, vol.389, p.1-33.

Dyer B.C., Schanz U., Ladner F., Häring M.O., Spillmann T. (2008). Microseismic imaging of a geothermal reservoir stimulation. *The Leading Edge*, p.856-869.

Evans K.F., Roth P. (1998). The state of stress in northern Switzerland inferred from earthquake seismological data and in-situ stress measurements. *Report prepared for the Deep Heat Mining (DHM) Project Basel on behalf of Geothermal Explorers Ltd.*, Pratteln, Switzerland, 26pp.

Faber S., Bonjer K.P., Brüstle W., Deichmann N. (1994). Seismicity and structural complexity of the Dinkelberg block, southern Rhine Graben. *Geophys. J. Int.*, vol.116, p.393-408.

Fäh D., Giardini D., Bay F., Bernardi F., Braunmiller J., Deichmann N., Furrer M., Gantner L., Gisler M., Isenegger D., Jimenez M.J., Kästli P., Koglin R., Masciadri V., Rutz M., Scheidegger C., Schibler R., Schorlemmer D., Schwarz-Zanetti G., Steimen S., Sellami S., Wiemer S., and Wössner J. (2003). Earthquake Catalogue Of Switzerland (ECOS) And The Related Macroseismic Database. *Eclogae geol. Helv. - Swiss J. Geosci.*, vol.96, p.219-236.

Ferry M., Meghraoui M., Delouis B., Giardini D. (2005). Evidence for Holocene palaeoseismicity along the Basel-Reinach active normal fault (Switzerland) : a seismic source for the 1356 earthquake in the Upper Rhine graben. *Geophys. J. Int.*, vol.160, p.554-572.

Ferry M. (2004). Adaptation of the palaeoseismological approach to local tectonic regime: comparative study of the intraplate Basel-Reinach fault, Switzerland and the interpolate North Anatolian fault, Turkey. *PhD thesis, ETH-Zürich, Diss. No.15537*, 162pp.

Fracassi U., Nivière B., Winter T. (2005). First appraisal to define prospective seismogenic sources from historical earthquake damages in southern Upper Rhine Graben. *Quaternary. Sci. Reviews*, vol.24, p.403-425.

Fraefel M., Densmore A., Schmid S.M. (2006). Geomorphic constraints on Quaternary tectonic activity in the Basel area. *4th Swiss Geoscience Meeting*, Bern.

Giardini D., Wiemer S., Fäh D., Deichmann N. (2004). Seismic Hazard Assessment of Switzerland, 2004. *SED Internal Report*, 82 pp., http://www.earthquake.ethz.ch/research/Swiss_Hazard/.

Golke M., Coblentz D. (1996). Origins of the European regional stress field. *Tectonophysics*, vol.266, p.11-24.

Güldenpfennig M., Loeschke J. (1997). Die Zone von Badenweiler-Lenzkirch - eine variskische Suturzone. In: Büchel, G. & Lützner, H. (Hrsg.): Regionale Geologie von Mitteleuropa - Schriftenreihe der deutsch. *Geol. Ges. 2*: 56-57.

Gürler B., Hauber L., Schwander M. (1987). Die Geologie der Umgebung von Basel mit Hinweisen über die Nutzungsmöglichkeiten der Erdwärme. *Beitrag zur Geologischen Karte der Schweiz*, Lieferung 160.

Hann H.P., Sawatzki G. (2000). Neue Daten zur Tektonik des Südschwarzwalds. *Jahresberichte und Mitteilungen des oberrheinischen geologischen Vereins*, vol.82, p.363-376.

Hann H.P., Loeschke J., Frisch W., Sawatzki G., Vaida M. (2000). A Variscan suture zone in the Black Forest (South Germany). *Terra Nostra*, vol.1, p.1-50.

Häring M.O., Schanz U., Ladner F., Dyer B.C. (2008). Characterisation of the Basel 1 enhanced geothermal system. *Geothermics*, doi:10.1016/j.geothermics.2008.06.002.

Hölker A., Graf R. (2005). Modelling the seismograms of micro-seismic events at potential observation stations for the evaluation of alternative observation network configurations. *Report prepared for the Deep Heat Mining (DHM) Project Basel on behalf of Geothermal Explorers Ltd.*, Pratteln, Switzerland, 32 pp.

Huggenberger P., Dresmann H. (2009). Datenlieferung an die SERIANEX Group im Zusammenhang mit der Risikoanalyse zur Geothermiebohrung Basel 1 (26. März 2009). BGA Region 11. 7 pages, 3 maps.

Käser B., Kalt A., Borel J. (2007). The crystalline basement drilled at the Basel-1 geothermal site. A preliminary petrological-geochemical study. *Report to Geopower Basel AG for Swiss Deep Heat Mining Project Basel*. Institut de Géologie et d'Hydrogéologie, Université de Neuchâtel, Switzerland, 84pp.

Kastrup U., Zoback M.L., Deichmann N., Evans K., Giardini D. (2004). Stress field variations in the Swiss Alps and the northern Alpine foreland derived from inversion of fault plane solutions. *J. Geophys. Res.*, 109(B01402), doi:10.1029/2003JB002550.

Kock S. (2008). Pleistocene Terraces in the Hochrhein area – formation, age constraints, and neotectonic implications. *PhD thesis, Basel University*, 110pp.

Ladner F., Schanz U., Häring M.O. (2008). Deep-Heat-Mining-Projekt Basel – Erste Erkenntnisse bei der Entwicklung eines Enhanced Geothermal System (EGS). *Bull. Angew. Geol.*, vol.13/1, p.41-54.

Lambert J., Winter T., Dewez T.J.B., Sabourault P. (2005). New hypotheses on the maximum damage area of the 1356 Basel earthquake (Switzerland). *Quaternary Sci. Rev.*, vol.24, p.383-401.

Larroque J.M., Laurent P. (1987). Evolution of the stress field pattern in the south of the Rhine Graben from the Eocene to the present. *Tectonophysics*, vol.148, p.41-58.

Laubscher H. (2007). The 1356 earthquake: what do we really know? *Bull. Angew. Geol.*, vol.12/1, p.21-27.

Laubscher H. (2001). Plate interactions at the southern end of the Rhine graben. *Tectonophysics*, vol.342, p.1-19.

Lopes Cardozo G.G.O., Behrmann J.H. (2006). Kinematic analysis of the Upper Rhine Graben boundary fault system. *J. Structural Geol.*, vol.28, p.1028-1039.

Lopes Cardozo G.G.O., Edel J.B., Granet M. (2005). Detection of active crustal structures in the Upper Rhine Graben using local earthquake tomography, gravimetry and reflection seismic. *Quaternary Sci. Rev.*, vol.24, p.339-346.

Mayer-Rosa D., Cardiot B. (1979). A review of the 1356 Basel earthquake: basic data. *Tectonophysics*, vol.53, p.325-333.

Meghraoui M., Delouis B., Ferry M., Giardini D., Huggenberger P., Spottke I., Granet M. (2001). Active Normal Faulting in the Upper Rhine Graben and Paleoseismic Identification of the 1356 Basel Earthquake. *Science*, vol.293, p.2070-2073.

Meyer B., Lacassin R., Brulhet J., Mouroux B. (1994). The Basel earthquake: which fault produced it? *Terra Nova*, vol.6, p.54-63.

Nivière B., Bruestle A., Bertrand G., Carretier S., Behrmann J., Gourry J.C. (2008). Active tectonics of the southeastern Upper Rhine Graben, Freiburg area (Germany). *Quaternary Sci. Rev.*, vol.27, p.541-555.

Pavoni N., Maurer H.R., Roth P., Deichmann N. (1997). Seismicity and seismotectonics of the Swiss Alps. *In Deep Structure of the Swiss Alps: Results of NRP20, pp. 241–250, eds Pfiffner, O.A., Lehner, P., Heitzmann, P., Mueller, S. & Steck, A.*, Birkhäuser, Basel.

Peters G. (2007). Active tectonics in the Upper Rhine Graben – Integration of paleoseismology, geomorphology and geomechanical modelling. *PhD thesis, Amsterdam University*, 298 pp.

Schanz U., Spillmann T., Häring M.O. (2008). Beurteilung des reservoirs Basel 1. Teil II: Mikroseismisches monitoring. *Endbericht, Geothermal Explorers Ltd*, Basel.

Schmid S.M., Slejko D. (2009). Seismic source characterization of the Alpine foreland in the context of a probabilistic seismic hazard analysis by PEGASOS Expert Group 1 (EG1a). *Swiss J. Geosci.*, DOI 10.1007/s00015-008-1300-2.

Schmid S.M., Kissling E. (2000). The arc of the western Alps in the light of geophysical data on deep crustal structure. *Tectonics*, vol.19/1, p.527-545.

Schwarz M., Henk A. (2005). Evolution and structure of the Upper Rhine Graben: insights from three-dimensional thermomechanical modeling. *Int. J. Earth Sci.*, vol.94, p.732-750.

Spottke I., Zechner E., Huggenberger P. (2005). The southeastern border of the Upper Rhine Graben: a 3D geological model and its importance for tectonics and groundwater flow. *Int. J. Earth Sci.*, vol.94, p.580-593.

Tesauro M., Hollenstein C., Egli R., Geiger A., Kahle H.G. (2005). CGPS and broad-scale deformation across the Rhine Graben and the Alps. *Int. J. Earth Sci.*, vol.94, p.525-537.

Thury M., Gautschi A., Mazurek M., Naef H., Voborny O., Vomvoris S., Wilson W.E. (1994). Geology and hydrogeology of the crystalline basement of northern Switzerland. *Nagra Technical Report NTB 93-01*, Nagra, Wettingen, Switzerland.

Ustaszewski K. (2004). Reactivation of pre-existing crustal discontinuities: the southern Upper Rhine Graben and the northern Jura Mountains – a natural laboratory. *PhD thesis, Basel University*, 176 pp.

Vaida M., Hann H.P., Sawatzki G., Frisch W. (2004). Ordovician and Silurian protolith ages of metamorphosed clastic sedimentary rocks from the southern Schwarzwald, SW Germany: a palynological study and its bearing on the Early Palaeozoic geotectonic evolution. *Geological Magazine*, vol.141, p.629-643.

Valley B., Evans K. (2009). Stress orientation to 5 km depth in the basement below Basel (Switzerland) from borehole failure analysis. *Swiss J. Geosci.*, in press.

Vogt J. (1979). Les tremblements de terre en France. *Mem. B.R.G.M.*, vol.96, p.153-165.

Wells D.L., Coppersmith K.J. (1994). New Empirical Relationships among Magnitude, Rupture Length, Rupture Width, Rupture Area, and Surface Displacement. *Bull. Seism. Soc. Am.*, vol.84/4, p.974-1002.

Ziegler P.A., Dèzes P. (2007). Cenozoic uplift of Variscan Massifs in the Alpine foreland: Timing and controlling mechanisms. *Global and Planetary Change*, vol.58, p.237-269.

Ziegler P.A., Dèzes P. (2005). Evolution of the lithosphere in the area of the Rhine Rift System. *Int. J. Earth Sci.*, vol. 94, p.594-614.